THE ASTROPHYSICAL JOURNAL, 438:680–694, 1995 January 10

HUBBLE SPACE TELESCOPE FAR-ULTRAVIOLET IMAGING OF M31, M32, AND NGC 205

F. BERTOLA,[1] A. BRESSAN,[2] D. BURSTEIN,[3] L. M. BUSON,[4] C. CHIOSI,[5] AND S. DI SEREGO ALIGHIERI[6]

Received 1994 March 21; accepted 1994 July 19

ABSTRACT

Hubble Space Telescope Faint Object Camera (FOC) f/48 images of M31, M32, and NGC 205 (field of view 23″ × 23″ with 0.″45 pixel size) are analyzed as observed through the combined UV filters F150W and F130LP. The absolute calibration of the data and the internal disagreement between observed and expected count rates in the UV region lead us to suggest that the filter combination F150W + F130LP suffers from a 5 times degraded UV sensitivity. A corrected efficiency curve is constructed using the UV/optical spectral energy distributions of these three galaxies, which is consistent with all of the data analyzed here.

Eighty-one individual stars are detected in M31, 10 stars in M32, and 78 stars in NGC 205. Comparisons with other UV images and optical images indicates that these stars are hot, UV-bright stars, even though our corrected efficiency curve suggests that flux from 1200–2450 Å contributes only 7% of the counts in M32, 19% in M31, and 60% in NGC 205. The morphology of the galaxies in our images is consistent with existing data. The complex nucleus of M31 as seen by Lauer et al. (1993) is confirmed; M32 has a generally smooth appearance and NGC 205 is dominated by a UV-bright, somewhat resolved nucleus.

Analysis of these data is done through the new, extensive stellar isochrones of Bertelli et al. (1994) and the population synthesis models of Bressan, Chiosi, & Fagotto (1994). This analysis shows that high-metal stars ($Z > 0.05$) evolve into UV-bright stars (P-EAGB, H-HB, and AGB-manqué stars) that are less luminous and cooler but are significantly longer lived than the P-AGB stars produced by stars with $Z < 0.05$. Moreover, the proportion of P-EAGB, H-HB, and AGB-manqué stars is also a function of age, with older stars of fixed mean metallicity having a higher proportion than younger stars. Hence, with either metallicity or age differences as an interpretation of the line-strength luminosity correlation for ellipticals, the high-metallicity "tail" of the stellar content of a galaxy can produce far-UV flux in much greater proportion than its actual proportion of galaxy mass. Separately, the UV-brightest stars in these stellar populations will be the shorter lived P-AGB stars and, hence, more readily observed in imaging observations such as ours.

The resulting model of the sources of far-UV flux is inherently composite, with the total UV flux from a stellar population both rapidly increasing and changing its mean spectrum with increasing mean metallicity (or mean age). This model is consistent with five pieces of observational evidence: (1) the correlation of UV-optical color with metallicity documented by Burstein et al. (1988) for early-type galaxies, (2) the low absolute UV flux from M32, (3) the apparent composite nature of UV flux from giant E's and the bulge of M31, as seen by the Hopkins Ultraviolet Telescope (HUT) spectral observations of Ferguson & Davidsen (1993), (4) our FOC observations of P-AGB stars that contribute a minority UV flux in M31, and (5) the possibility that ellipticals might have correlations of either age or metallicity with absolute luminosity (Faber, Gonzalez, & Worthey 1992).

Subject headings: galaxies: individual (M31, M32, NGC 205) — galaxies: stellar content — ultraviolet: galaxies

1. INTRODUCTION

It is well known that the stellar population of elliptical galaxies contain a hot stellar component that produces a turn-up in the ultraviolet spectral energy distribution (SED) for $\lambda \sim 2000$ Å, commonly referred to as a "UV-rising branch" (Code & Welch 1979; Bertola et al. 1980, 1986; Oke, Bertola, & Capaccioli 1981; Bertola, Capaccioli, & Oke 1982). As detailed in Burstein et al. (1988), the flux level of this turn-up, relative to the V-band flux, correlates with the optical absorption line index Mg_2, in the sense that the greater the strength of this index, the bluer the UV/optical color. This $(UV-V)$-Mg_2 correlation is opposite to that observed for visible and near-infrared colors.

The Hopkins Ultraviolet Telescope (HUT) spectrograph on Astro-1 has been able to extend our knowledge of the UV SEDs of ellipticals with high-quality observations to the Lyman limit of the two brightest far-UV sources among early-type stellar populations: M31 and NGC 1399 (Ferguson et al. 1991; Ferguson & Davidsen 1993). In their analysis, Ferguson & Davidsen show that the mean temperature of hot stars in M31 must be hotter ($T_{\rm eff} = 30{,}000$ K) than the mean temperature of stars in NGC 1399 ($T_{\rm eff} = 24{,}000$ K). Further analysis by Ferguson & Davidsen (1993) adds support to this interpretation, implying that more than one kind of hot stellar population is present in ellipticals, with the mix of stellar populations changing with mean metallicity. Ferguson & Davidsen

[1] Department of Astronomy, University of Padua, Vicolo Osservatorio 5, 35122 Padua, Italy; bertola@astrpd.pd.astro.it.
[2] Padua Astronomical Observatory, Vicolo Osservatorio 5, 35122 Padua, Italy; bressan@astrpd.pd.astro.it.
[3] Department of Physics and Astronomy, Box 871504, Arizona State University, Tempe, AZ 85287-1504; burstein@samuri.la.asu.edu.
[4] Padua Astronomical Observatory, Vicolo Osservatorio 5, 35122, Padua, Italy; buson@astrpd.pd.astro.it.
[5] Department of Astronomy, University of Padua, Vicolo Osservatorio 5, 35122 Padua, Italy; chiosi@astrpd.pd.astro.it.
[6] Arcetri Astrophysical Observatory, Largo E, Fermi 5, Florence, Italy; sperello@arcetri.astro.it.

(1993) make the point, made previously by several studies, that the UV SEDs of ellipticals are mostly due to old stars.

In absence of direct observations of the hot stars, Greggio & Renzini (1990) examine in detail three competing hypotheses for the origin of hot stars in early-type galaxies that can be made consistent with the SEDs of elliptical galaxies:

Young stars.—A low level of continuing star formation is formally consistent in SED with the UV-rising branch (e.g., Bruzual 1983; Burstein et al. 1988; Bica & Alloin 1987, 1988; Rocca-Volmerange 1989). The two problems with this interpretation are that it gives no straightforward explanation of the relation between $1550-V$ and Mg_2, and that the few early-type galaxies which show clear optical evidence of ongoing star formation (e.g., NGC 205) do not follow the $(1550-V)$-Mg_2 correlation for more normal appearing ellipticals.

Old, low-mass stars.—Evolved low-mass stars which are able to spend a significant fraction of their lifetimes at high enough UV luminosities and temperatures to satisfy the constraints imposed by the $(1550-V)$-Mg_2 relation and the HUT observations. As summarized by Greggio & Renzini (1990), there are four potential candidates:

1. Post–red giant branch (P-RGB) stars that can be generated by an unusually high rate of mass loss during the RGB phase and high values of changes of helium abundance with changes of metallicity (i.e., $\Delta Y/\Delta Z \geq 3$). Their existence is a matter of speculation because of the dependence of the turnoff mass on the age and metallicity as well as the possible dependence of mass-loss rate on the metallicity.

2. Hot horizontal-branch (H-HB) stars and their progeny, named AGB-manqué stars. Such evolution is thought to be typical of low-mass stars with [Fe/H] $\gg$ 0.0, which can spend a significant fraction of their He-burning phase at high effective temperatures and avoid the classical asymptotic giant branch (AGB) phase. This can be accomplished either with a suitable values of $\Delta Y/\Delta Z$ and strong dependences of the mass-loss rates on the metallicity (Greggio & Renzini 1990) or even with canonical mass-loss rates and suitable values of $\Delta Y/\Delta Z$ (Castellani & Tornambé 1991; Horch, Demarque, & Pinsonneault 1992; Dorman, Rood, & O'Connell 1993; Fagotto et al. 1994a, b; Fagotto 1994).

3. Post–early AGB (P-EAGB) stars. These stars undergo normal horizontal-branch evolution but depart from the AGB before the start of the thermally pulsed regime of the He-burning shell and eventually join the evolutionary scheme of the AGB-manqué stars.

4. The H- and He-burning post-AGB (P-AGB) stars. This has historically been considered the standard channel for producing sources of UV radiation from old stellar populations (Schönberner 1983; Burstein et al. 1988; Bertelli, Chiosi & Bertola 1989). These stars leave the AGB either during a thermal pulse (He-burning P-AGB) or between two pulses (H-burning P-AGB). As the body of evolutionary tracks for the He-burning scheme is very limited, most of the studies of the UV excess are based on the H-burning P-AGB stars. There are several drawbacks in the H-burning P-AGB scheme. In terms of the stellar evolutionary models, modeling the H-burning P-AGB phase depends entirely on the adopted relation between the mass of the core and the mass of the residual envelope (see Greggio & Renzini 1990 for details). Furthermore, the H-burning shell at the surface does not release enough energy to account for the strongest UV emissions (Greggio & Renzini 1990). Finally, there is the embarrassing result that the characteristic temperature of the H-burning P-AGB stars (similar remark applies also to the He-burning P-AGB mode) is too hot to explain the pronounced turnover near the Lyman limit in observed spectra (Ferguson et al. 1991; Ferguson & Davidsen 1993).

Binary stars.—Evolved binary stars with hot accretion disks have been suggested as a third possible source of hot stars in early-type galaxies (see Greggio & Renzini 1990). Owing to the complexity of this scheme, and the large number of possible connections of binary evolution to overall stellar populations, the effect of binary stars has not yet been considered.

Independent of the source (or sources) of the UV-rising branch in ellipticals, there are several scientific reasons for understanding the hot stellar populations in these galaxies. If these hot stars are old (where "old" here simply means not main-sequence OB stars), they provide basic clues toward understanding the post–giant branch evolution of low-mass stars. If there is a mix of hot stars that could change with age or metallicity, such a mix could very well change as a function of look-back time, affecting the appearance of galaxies at high redshift (see, e.g., the suggestion advanced by Bressan et al. 1994 about the potential use of the UV excess to date elliptical galaxies). Such an age/metallicity dependence could also be consistent with the interpretation of Faber et al. (1992) and Gonzalez (1993) that the line-strength/color–absolute magnitude correlation for gE's is as much age-driven as metallicity-driven (with the brighter gE's being older than the fainter gE's and dwarf E.s).

The fact that a reasonable case can be made that a mixture of hot stellar populations produces the UV-rising branch requires that spectroscopic observations be supplemented with direct measures of luminosity functions for these stellar populations. To make further progress, one needs to directly measure the fluxes and colors of the hot stars producing the UV-rising branch. This is the scientific goal of the *Hubble Space Telescope* (*HST*) Faint Object Camera (FOC) observations presented here. For our test objects we chose the old stellar populations that are both near enough for resolution into individual stars, and dense enough that individual hot stars could be expected to be detected—the nuclear regions of M31, M32, and NGC 205.

Our FOC observations are presented in § 2, in which the problems experienced with data reduction are quantitatively evaluated. Our imaging results on both the morphology of the host galaxy and the fluxes of the UV-bright point sources are discussed in § 3. An attempt to compare the fluxes of the observed point sources to predictions from stellar evolution theory and models of population synthesis is presented in § 4. Finally, the main conclusions of this paper are given in § 5.

2. OBSERVATIONS AND REDUCTION

2.1. *Observations*

The f/48 optical train of the *HST* FOC was used for the observations reported here. The observing configuration covered a field of 23″ × 23″ with 512 × 512 square pixels of size 0.″045. This field was centered on the nucleus of M32, but is off-center for M31 and NGC 205. In the case of M31, this offset was unintentional; in the case of NGC 205, the field was shifted by about 6″ to the southeast of the nucleus to avoid a bright star forming region. A combination of the FOC f/48 F150W broadband UV filter and the F130LP long-pass filter (to keep sky background due to geocoronal Lyα to a minimum) was

TABLE 1

LOG OF OBSERVATIONS

Object	Date	Exposure Time (s)	Exposures
NGC 205.....	1991 Oct 14	8177.5	5
M31.....	1991 Nov 27	8444.5	5
M32.....	1991 Nov 28	7037.6	4

used. (Observations planned with the F220W filter to provide UV colors for hot stars were not possible, owing to time limitations.)

A log of the observations is presented in Table 1. Within each set of exposures, the telescope was pointed in one position for two exposures, and then offset by 1″ for the other three exposures (one exposure of M32 was corrupted). This was done to reduce the effects of reseau marks and blemishes on the final image. The data for each individual exposure were flat-fielded and geometrically corrected using the standard pipeline reduction at the STScI and subsequently reduced with the IRAF/STSDAS package.

The frames of each object were registered and co-added, then the background was subtracted in the following way: the co-added image of NGC 205 exhibits only point sources (including a bright, nearly stellar nucleus) superimposed on a uniform background. As such, we have fitted a constant value to regions free of stars for this image, and obtain a background count rate of 0.00138 counts s^{-1} $pixel^{-1}$. This count rate is actually lower than the predicted detector background measured in orbit outside the South Atlantic Anomaly (0.002 counts s^{-1} $pixel^{-1}$; Greenfield et al. 1991). Although the NGC 205 image was taken 1.5 months earlier than those of M31 and M32, we find that the count rate measured in the M32 image near the edge is also comparable to this value. Moreover, Windhorst & Keel (1994) report an FOC background rate of 0.00145 counts s^{-1} $pixel^{-1}$ on exposures taken within 2 months of our exposure, within mutual errors the same measurement as our own. Hence, we feel justified in using a background rate of 0.00138 counts s^{-1} $pixel^{-1}$ for all three exposures. Figures 1*a*, 1*b*, and 1*c* (Plates 24, 25, and 26) present the FOC f/48 + F150W + F130LP images (*without* deconvolution) in both gray-scale forms and in terms of contour maps. The features on these images will be discussed in § 3.

TABLE 2

NGC 205 INDIVIDUAL SOURCES

X (pixels)	Y (pixels)	m_{15}	Δα	Δδ	X (pixels)	Y (pixels)	m_{15}	Δα	Δδ
38.5	53.1.....	19.32	−5.″63	3.″17	66.5	321.9.....	21.13	−2.94	−8.73
109.5	45.4.....	21.63	−2.49	3.90	97.5	288.7.....	21.38	−1.73	−7.07
83.7	79.6.....	20.81	−3.46	2.23	140.5	314.2.....	21.02	0.34	−7.99
186.5	38.8.....	19.94	0.93	4.60	192.6	304.4.....	21.03	2.62	−7.27
274.4	40.8.....	20.04	4.88	4.98	213.7	334.6.....	20.97	3.72	−8.51
402.4	68.7.....	20.30	10.76	4.41	216.9	344.8.....	21.60	3.92	−8.95
422.7	130.6.....	19.67	12.01	1.75	297.5	335.7.....	20.93	7.49	−8.12
329.5	101.6.....	20.74	7.67	2.55	286.1	332.6.....	22.42	6.96	−8.04
353.4	114.8.....	21.56	8.81	2.08	282.4	324.4.....	22.03	6.75	−7.69
368.2	127.3.....	21.75	9.54	1.60	228.5	375.4.....	21.56	4.60	−10.26
317.5	127.3.....	20.79	7.27	1.33	33.5	360.0.....	21.24	−4.22	−10.61
295.4	115.3.....	22.05	6.22	1.75	37.7	381.3.....	21.24	−3.92	−11.54
272.5	125.3.....	22.80	5.25	1.18	66.7	408.6.....	20.85	−2.47	−12.61
246.6	94.1.....	21.25	3.92	2.44	29.3	426.2.....	19.74	−4.06	−13.60
306.6	147.1.....	21.16	6.89	0.38	53.3	439.7.....	20.09	−2.91	−14.08
337.7	143.2.....	20.49	8.26	0.73	91.6	459.8.....	21.60	−1.08	−14.77
332.9	134.3.....	21.99	8.00	1.10	101.5	442.8.....	20.77	−0.73	−13.96
323.8	158.4.....	21.45	7.72	−0.03	152.4	463.8.....	20.29	1.66	−14.63
327.8	179.2.....	20.64	8.01	−0.94	163.0	408.3.....	21.33	1.84	−12.09
220.6	119.0.....	20.77	2.89	1.19	239.6	403.9.....	20.71	5.26	−11.48
154.0	137.6.....	16.46	0.00	0.00	191.1	446.9.....	20.99	3.31	−13.67
101.2	133.4.....	24.78	−2.39	−0.09	281.5	433.3.....	20.72	7.29	−12.57
114.9	136.2.....	20.86	−1.76	−0.15	310.6	394.3.....	20.48	8.38	−10.67
110.9	166.2.....	20.14	−1.78	−1.51	40.5	60.8.....	17.90	−5.50	2.84
145.4	192.1.....	20.24	−0.10	−2.49	78.1	88.4.....	23.09	−3.67	1.80
224.2	196.3.....	20.82	3.46	−2.26	52.1	78.8.....	21.17	−4.88	2.09
227.1	203.5.....	20.48	3.63	−2.57	51.4	73.2.....	21.73	−4.94	2.34
245.8	220.1.....	19.94	4.55	−3.21	215.6	97.0.....	21.29	2.54	2.15
295.0	216.6.....	19.99	6.74	−2.79	245.4	182.5.....	21.59	4.33	−1.53
304.5	237.9.....	20.16	7.28	−3.69	123.4	183.4.....	21.39	−1.13	−2.21
274.3	243.5.....	20.21	5.96	−4.11	170.0	147.8.....	20.19	0.77	−0.37
250.3	234.4.....	21.85	4.83	−3.83	391.5	184.5.....	21.38	10.89	−0.81
257.4	269.3.....	21.38	5.33	−5.35	350.7	264.9.....	21.25	9.49	−4.66
343.6	259.6.....	21.11	9.14	−4.46	245.4	182.5.....	21.59	4.33	−1.53
368.6	278.3.....	20.05	10.37	−5.16	415.0	472.4.....	21.04	13.48	−13.62
66.3	235.1.....	19.28	−3.41	−4.84	36.8	281.5.....	21.61	−4.49	−7.08
119.2	254.0.....	21.34	−0.94	−5.40	82.7	412.9.....	22.82	−1.73	−12.72
124.1	282.9.....	19.83	−0.57	−6.67	213.0	408.6.....	21.85	4.08	−11.83
149.3	294.5.....	19.28	0.63	−7.06	186.7	407.2.....	22.36	2.90	−11.91
53.5	303.4.....	21.67	−3.62	−7.97					

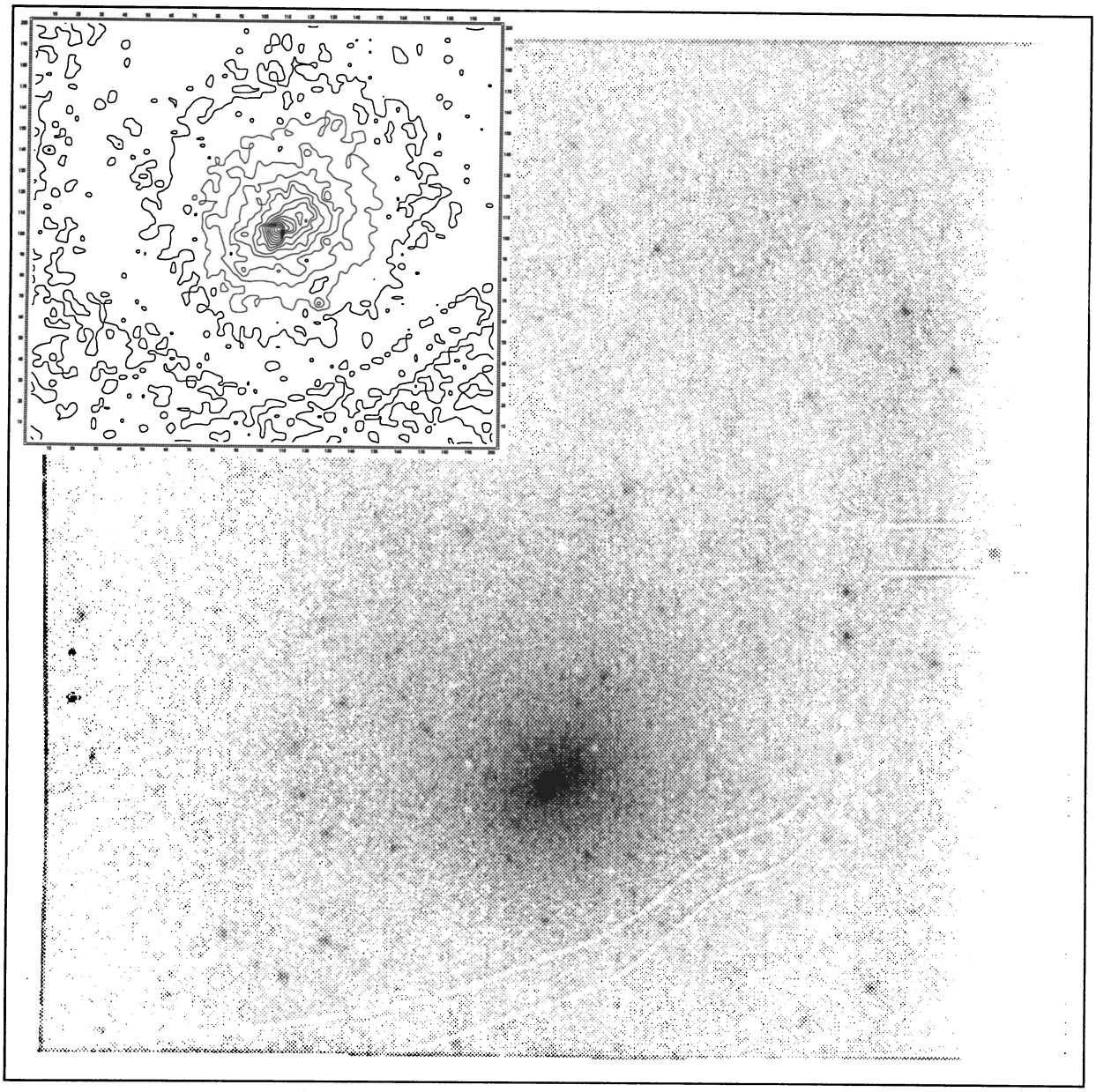

FIG. 1*a*

FIG. 1.—(*a*) FOC/48 image and contour map of the innermost region of M31. The vertical axis is rotated 98° counterclockwise from north. (*b*) FOC/48 image and contour map of the innermost region of M32. The vertical axis is rotated 122° counterclockwise from north. (*c*) FOC/48 image and contour map of the innermost region of NGC 205. The vertical axis is rotated 173° counterclockwise from north.

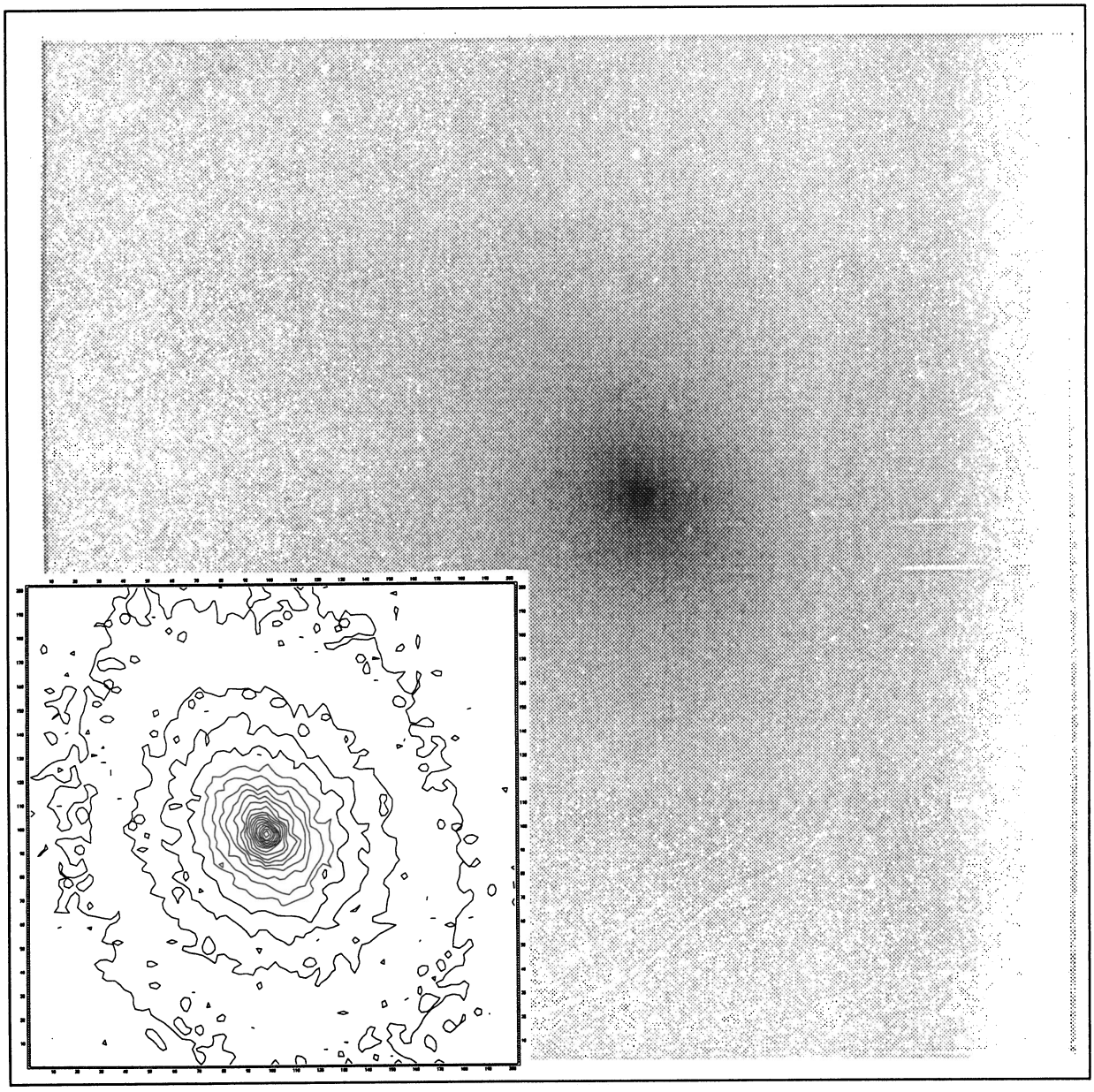

FIG. 1*b*

BERTOLA et al. (see 438, 682)

PLATE 26

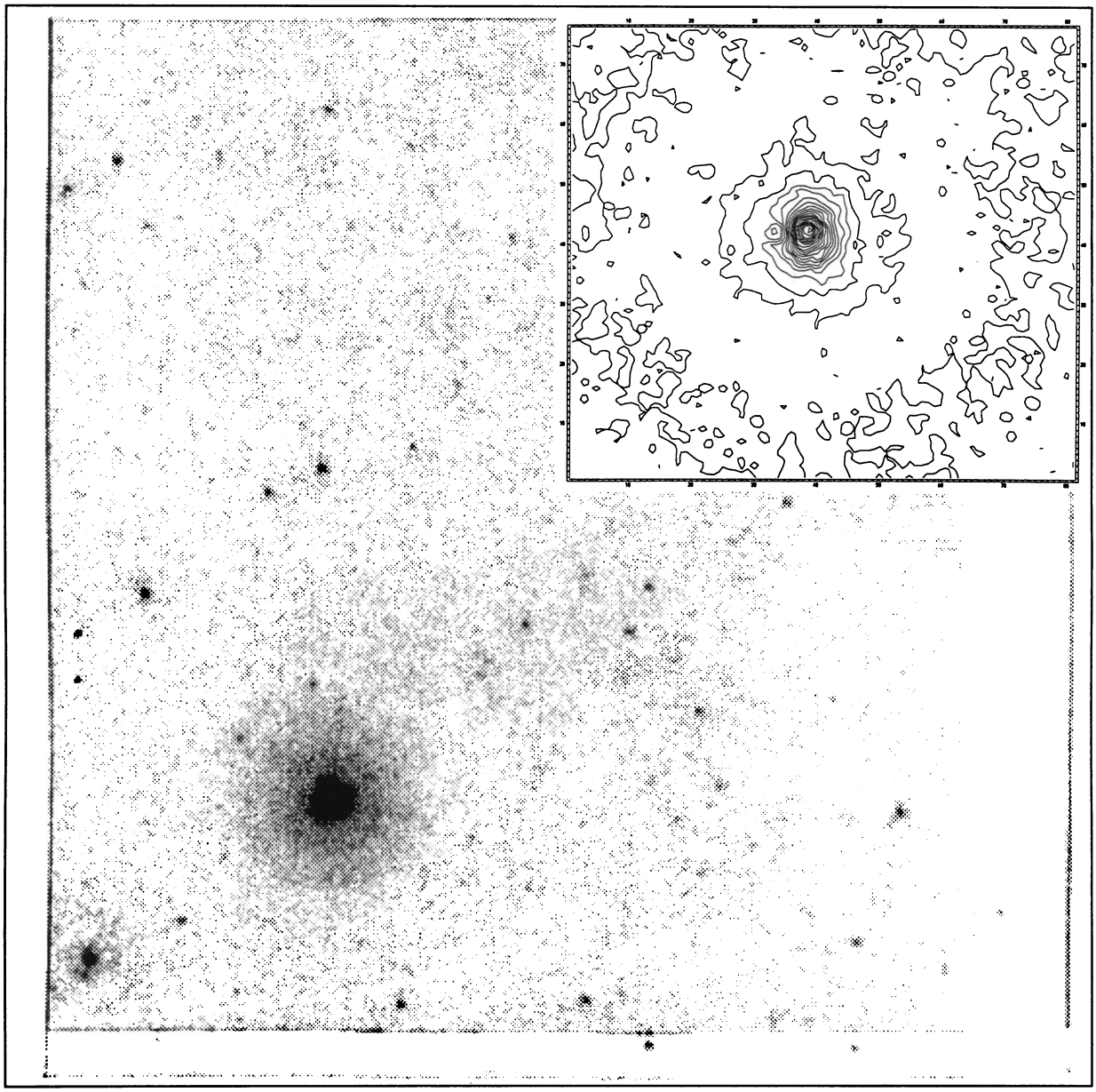

FIG. 1*c*

BERTOLA et al. (see 438, 682)

Stellar photometry is performed with the APPHOT package in IRAF, using a circular aperture with a radius of 4.5 pixels. The "sky" is measured in an annulus from 6 to 11 pixels radius. The resulting flux is then corrected for both the flux lost due to the extended wings of the aberrated point-source function (PSF), 1.86 mag, and the fact that the "sky" is measured in a region where the PSF has not gone to zero (0.24 mag; cf. discussion of King et al. 1992). We choose a magnitude scale such that a star with $m_{HST} = 19.09$ gives a count rate of 1, count s^{-1} from the fully corrected PSF, corresponding to a mean flux of 8.39×10^{-17} ergs cm^{-2} s^{-1} $Å^{-1}$. Magnitudes for all individual objects in each galaxy are given in Table 2 (NGC 205), Table 3 (M31, and Table 4 (M32), together with positional information. The corresponding luminosity functions are shown in Figure 2.

2.2. *Absolute Calibration*

While the F150W filter has a nominal peak wavelength of about ~1520 Å, it is also known to have a long tail of significant transmission toward the red (the "redleak"; see the FOC reference manual, Paresce 1992).

Therefore an absolute flux calibration can only be obtained by convolving the adopted total efficiency curve—filter efficiency × FOC efficiency × optical transfer function of *HST*—with the SED of the object to be calibrated. While the FOC efficiency and *HST* optical transfer function are known to within 10% from in-flight tests (Sparks 1991), the only efficiency curves for the F150W and F130LP filters available at the current time are based on ground-based measurements. We term this combined "nominal" efficiency curve $\Gamma^N_{15}(\lambda)$. As it is unlikely that a direct calibration will be made of this combination of filters that is more accurate than the one derived in this paper, we have proceeded with the following analysis.

We have three means of checking the reliability of $\Gamma^N_{15}(\lambda)$. All of these checks rely on descriptions of sensitivity or SEDs that themselves carry a nonnegligible degree of uncertainty. The most direct calibration method uses *IUE* fluxes measured for all three galaxies by Burstein et al. (1988) and Buson, Bertola, & Burstein (1990). From this comparison we derive a "corrected" total efficiency curve, $\Gamma^C_{15}(\lambda)$. The second method is also an internal check, using the apparent magnitude of a B main-sequence star in NGC 205 to compare predictions of $\Gamma^N_{15}(\lambda)$ and $\Gamma^C_{15}(\lambda)$. The third method is an external check, comparing our count rates to those made with the M31 FOC f/48 + F175W system by King et al. (1992) for stars observed in common (with data kindly provided by I. R. King and P. Crane). This last test can only differentially compare filter efficiencies, requiring also a knowledge of the FOC f/48 + F175W system efficiency for an absolute measurement.

2.2.1. *IUE-derived Calibration of Filter Efficiency*

To simulate the *IUE* aperture, we measure the total background-subtracted count rate within a square of side length 275.8 pixels, or an effective area of 154 arcsec^2, the same area as used by Burstein et al. (1988). The shape of the actual *IUE* aperture is not used for the following reasons. First, for both M31 and NGC 205, the nucleus is sufficiently offset that an aperture of 20″ × 10″ centered on the nucleus is too large for the image. Second, the *IUE* observations themselves are made at different position angles (Burstein et al. 1988). Third, centering of a galaxy within the *IUE* aperture is typically accurate to 1″–2″ (Burstein et al. 1988). We test the effect of using noncentered square apertures on our estimate of total counts with the *IUE* aperture in the following manner. For all three galaxies we measure the total counts in about ten 154 arcsec^2 apertures in different positions, all of which contain the nucleus but are shifted relative to each other. The resulting count rate within the *IUE* aperture is thus the mean of all these measurements and the error does not exceed 5%.

As the sensitivity of our filter-instrument-telescope combination extends from 1250 to 6000 Å, we require SEDs for these three galaxies over this wavelength region for convolution with the instrumental response function. These SEDs were constructed by combining UV fluxes measured with *IUE* (Burstein et al. 1988) with either optical ground-based measurements taken with an equivalent aperture for M31 and M32 (Oke et al. 1981) or a smooth interpolation in flux between 3200 Å and the *V* passband for NGC 205. The adopted full SEDs are shown in Figure 3, plotted as the logarithm of the absolute flux (in wavelength units) observed with the *IUE* aperture versus wavelength.

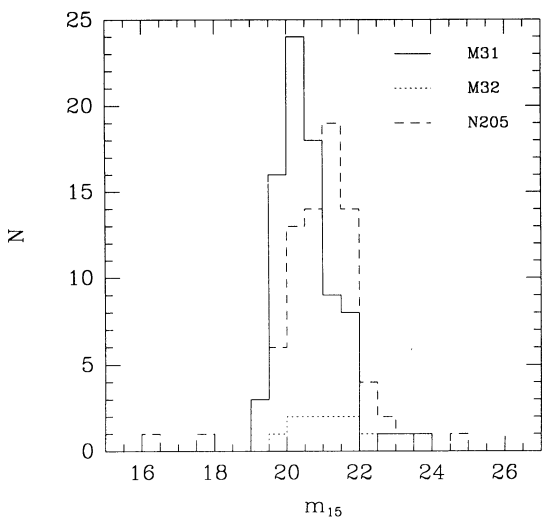

FIG. 2.—Luminosity functions of individual sources in M31, M32, and NGC 205

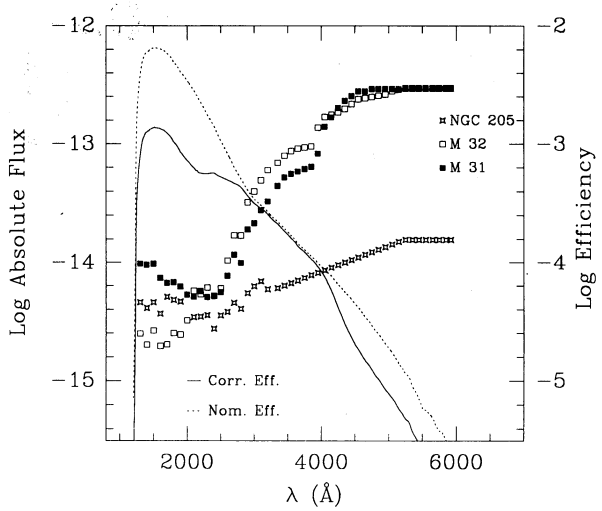

FIG. 3.—UV/optical SEDs of the three observed galaxies. Fluxes are expressed on a logarithmic scale. Both nominal efficiency (*dashed line*) and our own derived efficiency (*solid line*) of the system are superimposed.

TABLE 3

M31 INDIVIDUAL SOURCES

X (pixels)	Y (pixels)	m_{15}	$\Delta\alpha$	$\Delta\delta$	m_{17}	$m_{15}-m_{17}$
102.8	58.8.....	20.40	−4.″20	−6.″41	28.24	−7.84
102.3	93.0.....	21.41	−2.68	−6.64	...	...
107.1	312.4.....	20.55	7.17	−7.75	...	...
119.0	45.6.....	20.79	−4.70	−5.60	...	...
127.7	431.5.....	20.28	12.62	−7.56	28.68	−8.40
129.6	295.3.....	20.82	6.54	−6.64	...	...
130.2	39.2.....	19.81	−4.91	−5.06	28.05	−8.24
136.3	149.2.....	20.38	0.04	−5.46	27.90	−7.52
139.6	126.2.....	20.42	−0.97	−5.17	28.95	−8.53
142.5	313.3.....	20.23	7.42	−6.18	28.44	−8.21
148.8	208.6.....	20.50	2.77	−5.26	28.78	−8.28
151.4	107.4.....	20.16	−1.74	−4.53	28.36	−8.20
151.3	56.0.....	19.94	−4.03	−4.22	27.75	−7.81
157.4	169.0.....	19.87	1.06	−4.63	27.79	−7.92
156.6	284.7.....	20.33	6.23	−5.37	...	...
172.7	258.4.....	20.67	5.15	−4.49	28.90	−8.23
178.6	191.2.....	20.81	2.18	−3.82	28.22	−7.41
182.1	100.6.....	20.61	−1.85	−3.11	29.10	−8.49
182.2	314.0.....	20.43	7.69	−4.40	29.06	−8.63
189.9	349.4.....	21.22	9.32	−4.28	...	...
192.8	400.3.....	21.48	11.62	−4.45	29.09	−7.61
209.9	273.5.....	22.52	6.05	−2.92	...	...
216.2	250.6.....	20.27	5.06	−2.50	28.04	−7.77
237.0	159.6.....	19.58	1.12	−1.02	...	...
250.5	351.7.....	21.09	9.79	−1.58	...	...
254.0	66.5.....	20.46	−2.94	0.31	28.23	−7.77
258.8	221.3.....	20.92	4.01	−0.42	...	...
262.5	353.6.....	21.44	9.95	−1.05	...	...
264.6	434.9.....	20.91	13.60	−1.45	28.59	−7.68
268.5	169.4.....	19.97	1.75	0.33	...	...
273.5	97.6.....	19.67	−1.43	0.99	27.78	−8.11
280.9	182.5.....	19.79	2.41	0.81	27.94	−8.15
283.9	260.2.....	20.58	5.91	0.47	28.17	−7.59
288.4	26.8.....	21.98	−4.51	2.09	...	...
290.6	270.9.....	20.45	6.42	0.70	28.30	−7.85
292.7	309.2.....	21.64	8.15	0.56	...	...
293.6	97.4.....	20.35	−1.32	1.89	...	...
295.7	79.9.....	20.25	−2.09	2.09	28.70	−8.45
304.9	385.3.....	20.03	11.63	0.65	28.15	−8.12
307.7	215.0.....	20.42	4.03	1.81	...	...
308.9	65.4.....	20.20	−2.66	2.77	28.72	−8.52
35.8	210.5.....	20.01	2.17	−10.33	28.22	−8.21
354.6	196.4.....	20.74	3.48	4.02	28.76	−8.02
358.2	267.0.....	20.77	6.66	3.75	...	...
369.7	409.3.....	21.70	13.09	3.40	...	...
376.5	20.0.....	20.48	−4.28	6.07	28.44	−7.96
377.3	317.1.....	20.05	9.02	4.30	28.48	−8.43
385.6	106.5.....	20.58	−0.35	5.95	...	...
391.6	145.1.....	20.71	1.41	5.98	28.26	−7.55
393.6	408.5.....	21.59	13.20	4.48	...	...
395.2	202.6.....	19.41	4.00	5.80	27.74	−8.33
394.9	224.4.....	19.66	4.98	5.65	28.37	−8.71
41.1	144.1.....	20.20	−0.76	−9.69	28.56	−8.35
407.3	36.0.....	20.06	−3.38	7.35	28.10	−8.04
422.0	356.7.....	19.67	11.06	6.06	28.11	−8.44
427.8	71.6.....	20.89	−1.66	8.05	...	...
432.0	240.2.....	21.25	5.91	7.21	...	...
436.5	190.3.....	19.81	3.70	7.72	27.83	−8.02
444.5	329.7.....	19.88	9.99	7.23	28.67	−8.78
448.6	457.5.....	19.84	15.73	6.64	28.61	−8.77
47.4	12.8.....	20.87	−6.60	−8.61	28.12	−7.25
48.4	226.2.....	21.52	2.95	−9.86	...	...
74.6	64.4.....	23.16	−4.12	−7.70	...	...
77.0	30.2.....	20.64	−5.64	−7.39	...	...
80.5	332.8.....	19.41	7.92	−9.07	27.13	−7.72
81.0	398.7.....	21.16	10.87	−9.45	...	...
81.9	63.5.....	21.72	−4.12	−7.37	...	...
98.4	212.7.....	20.77	2.65	−7.54	...	...
433.0	356.8.....	20.91	11.13	6.55	28.44	−7.53
311.8	269.3.....	21.55	6.48	1.66	29.05	−7.50
78.4	39.5.....	23.65	−5.21	−7.38	...	...
197.5	157.1.....	19.92	0.77	−2.77	28.04	−8.12
226.6	135.0.....	19.70	−0.04	−1.33	28.08	−8.38
237.3	95.6.....	20.18	−1.74	−0.62	28.31	−8.13
241.6	114.1.....	19.85	−0.89	−0.53	27.86	−8.01
240.6	129.4.....	19.28	−0.21	−0.67	...	...
262.1	152.6.....	19.55	0.96	0.15	27.96	−8.41
331.2	54.4.....	21.23	−3.01	3.83	28.78	−7.55
418.9	214.0.....	21.51	4.46	6.79	...	...
260.8	181.6.....	21.34	2.25	−0.08	...	...
353.8	237.8.....	20.15	5.33	3.73	...	...

All three galaxies have equally well defined *IUE* SEDs, with an absolute accuracy estimated to be at least 10% overall (Bohlin & Holm 1980). The optical SEDs of M31 and M32 obtained by Oke et al. (1981) were constructed to match the *IUE* fluxes, and we expect the overall SEDs for these galaxies to be accurate to 15%. The SED for NGC 205 is less accurate, owing to two factors. First, the *IUE* observations of NGC 205 were taken at orthogonal position angles for the SWP camera (1250–1950 Å) and for the LWR cameras (2000–3250 Å) (Burstein et al. 1988). As can be seen from the asymmetric distribution of UV-bright stars in this galaxy (Peletier 1993 and Fig. 1*c*), this probably means the fluxes in these two parts of the UV SED of NGC 205 refer to somewhat different stellar populations. Second, the optical SED for NGC 205 is an estimate made from its V-magnitude flux and its $B-V$ and $U-B$ mean colors. As a result, we believe a realistic estimate of the overall error in the SED of NGC 205 used here is 30%.

TABLE 4

M32 INDIVIDUAL SOURCES

X (pixels)	Y (pixels)	m_{15}	$\Delta\alpha$	$\Delta\delta$
62.6	317.5.....	21.10	−3.″68	−10.″14
144.2	279.7.....	20.51	−3.15	−6.12
259.3	278.6.....	19.73	−0.41	−1.70
459.2	323.7.....	21.76	6.14	4.82
411.8	203.1.....	21.15	0.40	5.93
289.3	25.8.....	21.94	−9.32	5.55
243.4	217.3.....	20.16	−3.13	−0.83
264.2	168.0.....	22.43	−4.50	1.16
106.6	469.3.....	20.54	3.17	−12.13
250.4	425.7.....	20.26	4.98	−5.60

We first compare observed count rates within the FOC-synthesized *IUE* aperture to those predicted by convolving the galaxy SEDs with $\Gamma^N_{15}(\lambda)$. We find that the predicted counts disagree with those observed in a systematic manner that is correlated with UV/optical colors determined from *IUE* observations, $155-V$ (Burstein et al. 1988). These differences are summarized in Tables 5A and 5B. NGC 205, with the bluest $1550-V$ color yields the largest ratio of predicted to observed FOC counts (3.55; ratio of cols. [7] and [8], respectively, in Tables 5A and 5B), while M32, with the reddest $1550-V$ color, has the lowest ratio (1.46). M31, with a $1550-V$ color intermediate between these two galaxies, has an intermediate ratio of predicted to observed count rate (2.20).

TABLE 5

FOC/48 PREDICTED VERSUS MEASURED COUNT RATES (counts s^{-1})

OBJECT (1)	WAVELENGTH INTERVALS IN (λ/100) Å 12–18[a] (2)	18–24[a] (3)	24–32[a] (4)	32–42[a] (5)	42–60[a] (6)	TOT_P[b] (7)	TOT_M[c] (8)	$STARS_M$[d] (9)
A. F150W+F130LP: Nominal Efficiency Curve $\Gamma^N_{15}(\lambda)$								
M31	79.3	42.5	30.5	70.7	96.4	319.5	145.6	13.8
M32	22.6	36.3	45.7	100.9	86.8	292.4	200.6	1.1
NGC 205	41.8	27.7	10.5	7.3	4.3	91.7	25.8	23.2
B. F150W+F130LP: Corrected Efficiency Curve $\Gamma^C_{15}(\lambda)$								
M31	16.6	10.7	23.3	63.9	45.2	159.7	145.6	13.8
M32	4.8	9.3	37.9	92.5	40.5	185.0	200.6	1.1
NGC 205	8.8	6.6	7.9	6.8	2.0	32.1	25.8	23.2
C. F175W:[e] Nominal Efficiency Curve $\Gamma^N_{17}(\lambda)$								
M31	44.8	49.6	19.0	34.4	4.4	192.2	256.0	13.0
D. F175W:[e] Corrected Efficiency Curve $\Gamma^C_{17}(\lambda)$								
M31	13.0	19.8	26.0	73.0	122.9	254.0	256.0	13.0

[a] Predicted count rate within the FOC-synthesized *IUE* aperture in the specified wavelength range as a function of the adopted filter combination and efficiency curve.

[b] Total predicted count rate within the FOC-synthesized *IUE* aperture as a function of the adopted filter combination and efficiency curve.

[c] Total measured FOC count rate within an aperture of 154 $arcsec^2$ as a function of the chosen filter combination.

[d] Measured FOC count rate of the resolved stars alone with an aperture of 154 $arcsec^2$ as a function of the chosen filter combination.

[e] King et al. 1992.

Whatever the source of depressed count rate in the FOC f/48+F150W+F130LP system, it is clear that the spectral sensitivity of our images is affected more in the UV than in the optical. Fortunately, the *IUE* fluxes of the three galaxies we observed permit a relatively crude approximation of the in-flight sensitivity function of our system. We have estimated a wavelength-dependent correction factor to be applied to $\Gamma^N_{15}(\lambda)$ to transform this efficiency curve into a corrected efficiency curve, $\Gamma^C_{15}(\lambda)$ that brings the *HST* and the *IUE*-optical data into reasonable agreement. It should be noted that this correction curve is not uniquely determined and the agreement obtained is not perfect, although well within the measurement errors. One source of scatter is the UV (1500–2500) color gradients observed in the inner 10″ of M31 and M32 by O'Connell (1992). Owing to the slight mismatch of the *IUE* aperture and FOC field such gradients could affect the *HST*/*IUE* comparison at the level of a few percent.

The multiplicative correction factors applied to $\Gamma^N_{15}(\lambda)$ to produce $\Gamma^C_{15}(\lambda)$ are 0.21 for $\lambda \leq 2000$ Å, monotonically increasing from 0.25 at $\lambda = 2200$ Å to 0.92 at $\lambda = 3000$ Å, to 0.95 $\lambda \sim 3200$–3800 Å, decreasing from 0.90 at $\lambda = 4000$ Å to 0.50 at $\lambda = 4400$ Å, and finally settling to 0.42 in the range $\lambda = 4800$–6000 Å. Our calculations indicate that changes in these corrections larger than ~20% over a wavelength region of 500 Å or more would push the FOC-*IUE* agreement outside of our estimated errors. The main feature of $\Gamma^C_{15}(\lambda)$ is the remarkable depression in the UV which reflects the obvious decreased UV transmission of the filter(s). Both the nominal total sensitivity efficiency of our FOC f/48+F150W+F130LP system, $\Gamma^N_{15}(\lambda)$, and the corrected efficiency, $\Gamma^C_{15}(\lambda)$, are shown in Figure 3, displayed over the SEDs of the three galaxies for reference.

Also given in Tables 5A and 5B are the count rates detected in resolved stars, $Stars_M$ *contained within the IUE aperture.* As is evident, within the observational errors all of the flux measured within the *IUE* aperture in the NGC 205 image comes from resolved stars, while stars contribute 9.5% of the flux in M31 and only 0.6% of the flux in M32.

To evaluate the contributions of these stars *to the UV fluxes* of these galaxies, one has to estimate how the observed *total* FOC count rate splits up into the UV and optical (redleak-generated) wavelength bands. Our estimate is given in Table 5B, which contains for each galaxy—besides the total expected count rate—the partial count rate expected in several regions of the spectrum as obtained with our corrected efficiency curve $\Gamma^C_{15}(\lambda)$. In the following sections of this paper we will refer to this information to estimate the fraction of the UV flux contributed by the resolved stars.

For comparison purposes Table 5A lists the same predictions that would be derived also from the nominal efficiency, $\Gamma^N_{15}(\lambda)$. It should be clear the rather dramatic difference that is made in the predicted UV contribution of the detected stars to our image between the nominal efficiency $\Gamma^N_{15}(\lambda)$ and our corrected efficiency, $\Gamma^C_{15}(\lambda)$.

2.2.2. *B0 V Star in NGC 205*

The brightest star (excluding the nucleus) in our image of NGC 205 is star No. 65, with $m_{15} = 17.9$ (Table 2). This star corresponds to star No. 4 in the list of bright blue stars in NGC 205 given by Peletier (1993), for which he measured $U = 19.24 \pm 0.10$, $B = 20.79 \pm 0.30$, and $U - B = -1.55 \pm 0.32$. Given the known ongoing star formation in NGC 205 (see Burstein et al. 1988; Peletier 1993), it is natural to interpret this as a young OB main-sequence star. With a galactic reddening of $E_{B-V} = 0.035$ (Burstein & Heiles 1984) and a distance modulus of 24.7 (Price & Grasdalen 1983), this star has $M_B = -4.12 \pm 0.2$, corresponding to a typical B0 V star. Convolving

the *IUE*-derived SED of B0 V stars with $\Gamma^N_{15}(\lambda)$ and placing it at the distance and reddening of NGC 205, m_{15} is predicted to be 15.9, 2 mag brighter than what is observed and well outside the errors of observations. In contrast, use of the corrected efficiency, $\Gamma^C_{15}(\lambda)$ predicts $m_{15}=17.7$, within these known errors. This comparison adds further support to our use of the corrected, UV-deficient, efficiency for our observations.

2.2.3. *Comparison with F175W Observations of M31 Hot Stars*

A direct comparison can be made, on a star-by star basis, of the magnitudes m_{15} measured in our image of M31 with the F175W observations of King et al. (1992) of M31. Through the kind efforts of I. King and P. Crane, we have been able to ascertain that, for 48 stars in common, the count rate in the F175W filter system is 1.47 times the count rate in the F150W+F130LP filter system. In both our observations and those of King et al. (1992), the stars detected are ~ 50 times brighter than the background. As also pointed out by King et al. (1992), such bright stars have not been seen in visible images of the center of M31 and are almost certainly UV-bright.

If one convolves the energy distribution of a star having an effective temperature of 25,000 K (a reasonable estimate for a typical UV-bright star in M31) with the nominal total efficiency of the F175W system (Γ^N_{17}) and of the F150W+F130LP system (Γ^N_{15}), one predicts a ratio (King et al. vs. this paper) of 0.7 in star counts. Instead, using Γ^N_{17} and Γ^C_{15}, owing to the depression of our adopted efficiency curve in the UV, the above ratio becomes 2.9. This latter value is about twice the observed value. We will see later that there are good reasons to slightly modify Γ^N_{17} too, in such a way that the new ratio reasonably matches the observed one.

3. MORPHOLOGY

NGC 205.—The nucleus of this galaxy appears barely resolved and slightly elongated (Fig. 1*c*). Gaussian profiles matching the nuclear profile have $\sigma_x=2.23$ pixels and $\sigma_y=2.70$ pixels, instead of the value $\sigma=1.4$ pixels that has been measured for a starlike object. Upon convolution with the predicted instrumental profile, one can derive an intrinsic angular size (FWHM) of $0''.8\times 0''.24$ which, adopting a distance of 710 kpc, gives an intrinsic linear size of 0.6×0.8 pc. The very blue color of the nucleus in the optical (Peletier 1993), combined with the brightness of $m_{15}=16.5$ and physical extent seem to indicate that it probably consists of a compact clump of young stars. If the young stars in this clump are of equal UV brightness as the individual hot stars seen elsewhere in this galaxy, ~ 10 stars are enough to account for the observed UV flux from the nucleus. Separate from the nucleus, 78 individual stars are observed spread out over the image. Within the statistical uncertainty, their radial distribution appears essentially uniform (Fig. 4), with a possible excess in the innermost region (5″ diameter). The whole count rate measured from NGC 205 is consistent with that integrated from individual stars and the nucleus (Table 5A); no diffuse UV component is detected.

M32.—The isophotes of the nuclear region of M32 in our image appear elongated, although regular in shape and becoming increasingly roundish toward the center (Fig. 1*b*). Only 10 individual stars are seen, apparently randomly distributed over the inner 30″ of this galaxy. Given the decreased UV sensitivity of our FOC observations it is of interest whether any of these stars might be detectable in the optical. Observations by Freedman (1989, 1992) and others indicate that the brightest stars resolved in M32 are very red AGB stars which will be too faint to be observed in the far-UV. Hence it is reasonable to assume that the 10 stars observed in M32 are, indeed, hot stars detectable only in the far-UV. These stars do belong to M32, as the lack of stars younger than 5×10^9 yr reported by Freedman (1989) allows us to rule out a possible contamination by the M31 disk population. The low number of UV-bright stars is consistent with the low UV flux in this galaxy, which has the reddest $1550-V$ color among the ellipticals studied by Burstein et al. (1988). Indeed, the low *IUE* flux of this object prevents us from significantly disentangling the relative UV contribution of stars and a possible diffuse component.

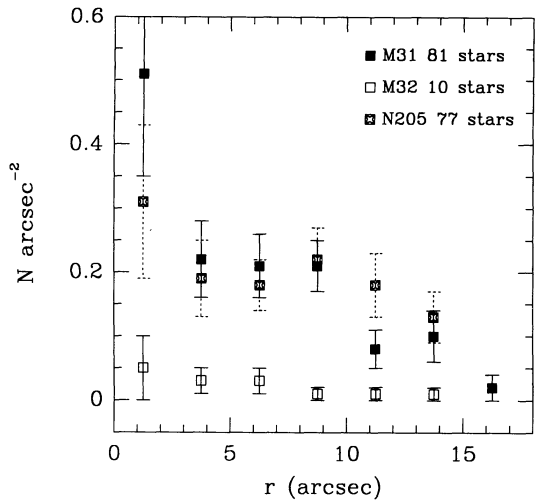

FIG. 4.—Surface density of individual sources in M31, M32, and NGC 205 as a function of radius.

M31.—The morphology of the innermost ($r<0''.8$) nuclear region of M31 appears complex (Fig. 1*a*), appearing to be an elongated source including a secondary compact region. This is consistent with a two-component structure for the M31 center region as proposed by Lauer et al. (1993). This agreement is perhaps not surprising, given the fact that nearly 70% of the flux in our F150W+F130LP observation comes from photons with wavelengths longer than 3200 Å.

In our FOC f/48 image of M31, 81 individual sources are detected, superimposed on strong, diffuse emission. All appear to be point sources, within the limitations of the variation of the PSF across the field. Unlike the stars observed in NGC 205 and M32, their concentration within a radius of 2″.5 appears significantly higher than in the rest of the field (Fig. 4), and the overall distribution appears regularly declining outward. Since the light coming from unresolved objects is due primarily to the redleak region (see below), we are prevented from directly comparing the relative contribution to the UV flux of hot resolved stars and the diffuse hot component as a function of radius.

As discussed earlier (§ 2.2.1) these hot stars contribute only 9.5% of the observed count rate within the *IUE* aperture (Tables 5A and 5B) or 13.8 counts s^{-1}. Of the 81 stars detected over the whole image (as opposed to 41 stars detected within the *IUE* aperture), 48 are also seen in the F175W observation of M31 obtained by King et al. (1992). Attempts to match individual sources in our image either with known globular clusters (Wirth, Smarr, & Bruno 1985) or known planetary nebulae (Ford & Jacoby 1978) reveal no convincing optical counterparts to any of these stars. The face that these stars are not seen in the optical is strong evidence that these are, indeed,

UV-bright objects. Compared to the UV luminosity function of NGC 205, the luminosity function of the detected sources in M31 (Fig. 2) appears narrower, more symmetric, and centered at a slightly brighter magnitude.

If we model the stars in M31 as having the SED of stars with $T_{\rm eff} > 25{,}000$ K, we estimate that at least 12 out of 14 counts s^{-1} fall in the 1200–2450 Å wavelength region. On the basis of the SED of M31 and $\Gamma^c_{15}(\lambda)$, the predicted count rate for our FOC observation in the 1200–2450 Å region is 27.3 ± 5 counts s^{-1} (taking into account measurement and calibration errors). This compares to the observed count rate from stars of 13.85 counts s^{-1}, of which 11.9 are from 1200–2450 Å. The formal ratio of counts from stars to total counts in the UV is 44^{+12}_{-9}% by these numbers, implying that about 50% of the flux in the far-UV is predicted to come from unresolved objects.

It should be emphasized that the UV count rate from the individual hot stars is reliably determined, owing to the fact that their non-UV emission is small. However, this is not true for the total UV count rate estimated for the *IUE* aperture, as this count rate is a small fraction of the total observed count rate (10%). A 50% error in this fraction (say, making it 25%) would decrease the stellar contribution from 44% to 29%, yet such an error cannot be ruled out with high significance. Hence, in the rest of this paper, while we will quote a predicted contribution of 50% of the individual stars to the total UV light, in reality this ratio could be anywhere from 30% to 70%.

4. THEORETICAL ANALYSIS

To analyze the evolutionary scenarios in which hot luminous stars of old age can be present we made use of the large grids of isochrones calculated by Bertelli et al. (1994), the models of population synthesis for elliptical galaxies presented by Bressan et al. (1994), and the grids of isochrones in the UV passbands of *HST* calculated by Chiosi et al. (1994) to study the color-magnitude diagram (CMD) of 47 Tuc obtained by Paresce et al. (1991) and De Marchi, Paresce, & Ferraro (1993). The libraries of stellar tracks and isochrones in usage contain all the evolutionary stages from the main sequence to the most advanced stages (white dwarfs or carbon-ignition depending on the stellar mass) and encompass a wide range of chemical composition. The key points of the technique used to derive magnitudes and colors in UV passbands of *HST* are summarized below for the sake of better understanding.

Of particular relevance to the present paper is that various possible old and young stellar populations have been included in the evolutionary stellar population models made by Bressan et al. (1994), so that accurate predictions can be made for the kinds of stars possibly responsible for the UV flux.

As M31 has both F150W and F175W images available, much of the analysis will concentrate on interpreting these data and the derived CMD. For the following discussion we assume that the typical age of old stellar populations in M31 is 13×10^9 yr. Taking into account the slow evolution of the related CMD diagram, much of the same results would apply if the age were between 7 and 15×10^9 yr. The less UV-constrained stellar populations of M32 (with no detectable UV excess) and NGC 205 (with ongoing star formation) will be explored separately.

4.1. *Theoretical HST UV Magnitudes*

According to the core aperture photometry technique, *HST* instrumental magnitudes are defined as (§ 2.2; Paresce et al. 1991; De Marchi et al. 1993):

$$m_i = -21.1 - 2.5 \log \left(\frac{(F_i - BA)U_i}{\epsilon t} \right), \quad (1)$$

where i stands for the particular passband in use, F_i is the total number of counts within the aperture radius (approximately equal to the half-width at half-maximum of the PSF), B is the background value within a suitably chosen annulus centered on each star peak, A is the aperture area, t is the exposure time, ϵ is the fraction of energy falling into the core aperture with respect to that in the annulus, and U_i is the inverse sensitivity of the instrument mode used (camera + filter) expressed in ergs cm^{-2} $Å^{-1}$. The quantity $(F - BA)/\epsilon t$ corresponds to the count rate detected by the instrument.

The corresponding theoretical count rates N^i_c (counts s^{-1}) for any passband i in use are derived as follows. First we calculated the absolute count rates

$$N^i_c = \Sigma \int_{\lambda_{\rm min}}^{\lambda_{\rm max}} [S(\lambda)/(hc/\lambda)]\Gamma_i(\lambda) d\lambda \, . \quad (2)$$

In the above relation, $S(\lambda)$ is the spectral energy distribution coming from an ideal star located at 10 pc with $\log L/L_\odot = 0$ and given $\log T_{\rm eff}$, gravity, and composition. $\Gamma_i(\lambda)$ is the combined quantum efficiency that we have already presented above, and Σ is the area of the collecting surface $\simeq 39{,}000$ cm^2. Furthermore, h is the Planck constant and c is the speed of light in the appropriate units. The integral is calculated from $\lambda_{\rm min}$ to $\lambda_{\rm max}$, the wavelengths of the first and last nonzero values for $\Gamma_i(\lambda)$.

The spectral flux $S(\lambda)$ is expressed in ergs cm^{-2} s^{-1} $Å^{-1}$. The theoretical $S(\lambda)$ are obtained from the Kurucz (1992) library of stellar spectra and normalized to the solar luminosity and the distance of 10 pc. We note that N^i_c varies with the metallicity, $T_{\rm eff}$, and gravity of the stars studied, i.e., across the CMD.

Finally, the absolute instrumental magnitude of a star with given $\log L/L_\odot$, $\log T_{\rm eff}$, and metallicity, when observed with a particular passband of the FOC is

$$M_i = -21.1 - 2.5 \log (U_i + L/L_\odot + N^i_c) \, . \quad (3)$$

The adopted U_i are $U_{15} = 8.39 \times 10^{-17}$ ergs cm^{-2} s^{-1} $Å^{-1}$ and $U_{17} = 7.65 \times 10^{-17}$ ergs cm^{-2} s^{-1} $Å^{-1}$, where the notation 15 refers to our FOC images and 17 refers to the F175W images of King et al. (1992), from which the calibration of U_{17} has been derived.

4.2. *M31: Observations versus Model*

4.2.1. *Evolutionary Model SEDs for M31*

Evolutionary stellar population models of the kind explored by Bressan et al. (1994) can give an indication of the kinds of UV luminosity functions produced by different kinds of stellar populations. For the following discussion, it is worth recalling that while P-AGB stars are always present in normal-metallicity stellar populations, the existence of P-EAGB, H-HB, and AGB-manqué stars is possible only if the metallicity and/or the ratio $\Delta Y/\Delta Z$ are greater than suitable threshold values. With the stellar and galaxy models used in this study the threshold values are $Z > 0.05$ and $\Delta Y/\Delta Z > 2.5$ (Fagotto et al. 1994a, b; Bressan et al. 1994).

Galaxy models with $1500 - V$ colors near 3.5 (Burstein et al. 1988) are selected for M31 which, according to the precepts in Bressan et al. (1994), have a total luminous mass of 1×10^{12}

$M_\odot$ and an age of 13×10^9 yr. For the sake of better understanding the effect of different kinds of hot old stars on the integrated SED of M31, results are explored from models with the same mass but three different abundance distributions: (1) A model that results from the closed-box approximation galaxy evolution and a star formation law that is a power law of the gas mass ($dM_g/dt = \nu M_g^\kappa$): This model predicts a distribution of stellar mass with metallicity that has an apparent excess of low-metallicity stars, relative to real galaxies (Bressan et al. 1994). (2) A modification of case 1, in which all of the stars with $Z > 0.05$ are assigned the $Z = 0.05$: This upper limit to the metallicity is meant to exclude the possibility that the UV excess is caused by P-EAGB, H-HB, and AGB-manqué stars (they can occur only if $Z > 0.05$) and to check whether the observed SED is compatible with the UV flux generated by the sole P-AGB stars (no metallicity threshold is required). (3) Another modification of case 1, in which all stars with $Z < 0.008$ are assigned the value $Z = 0.008$: This model is intended to mimic the effects of so-called infall models (Bressan et al. 1994).

The model results are presented in Figures 5*a* and 5*b* superimposed to the observed SED of M31 (Burstein et al. 1988; Oke et al. 1981). The theoretical SEDs and the observed one are normalized at 5550 Å. Among the computed models, case 1 (closed-box) and case 2 (without high-metallicity stars) have poor fits (Figure 5*a*); in particular, when the highest metallicity stars are forced to produce UV flux only via the P-AGB channel, the model predicts too low a UV flux. On the contrary, the theoretical SED of case 3 (without very metal-poor stars) gives a better fit to the observational SED of M31 (Fig. 5*b*). Although the present match has to be improved—possibly by exploring further the parameter space of the synthesis code—it gives strong support in favor of a population mix in which metal-rich stars prevail. Interestingly, in such a model the cumulative fractional mass of stars with $Z > 0.05$ is only about 10% of the total. Specifically, 7% of the stars have metallicities of $0.05 < Z < 0.06$ and 3% have $0.06 < Z < 0.07$. Apparently a minority of the stellar population can produce as much UV flux as the majority. This result can be explored in another way as well.

4.2.2. *Simple Stellar Population Models for M31*

Single stellar populations (SSPs) are models in which all of the input parameters of a coeval stellar population are specified except the initial mass function. To be consistent with the analysis of the SEDs above, the SSPs used here have an age of 13×10^9 yr. Separately, the mass-loss rates during the RGB and AGB stages are parameterized in terms of the parameter η, here chosen to be 0.45. In this connection one should be aware of the strict dependence of the UV populations predicted by the models on the detailed assumptions about envelope mass loss: in particular such assumptions will affect the relative contribution of the P-AGB and other hot star channels to the UV flux. SSPs with two limiting cases of metallicities are considered: $Z = 0.05$ is the upper limit of the bulk of stars contributing to the UV upturn only via the P-AGB channel (a marginal contribution from P-EAGB is also possible). $Z = 0.1$ is the upper limit to the metallicity of the much smaller fraction of stars contributing to the UV excess via P-EAGB, H-HB, and AGB-manqué channels.

The SEDs generated by these two SSPs expressed as the logarithm of the flux in units of $L_\odot$ Å^{-1} are shown in Figure 6. The SED plotted as a dotted line is for $Z = 0.05$, while the dashed line plots the SED for $Z = 0.1$. The color $1550 - V$ is found to be 5.4 for the $Z = 0.05$ SSP, while it is -1.58 for the

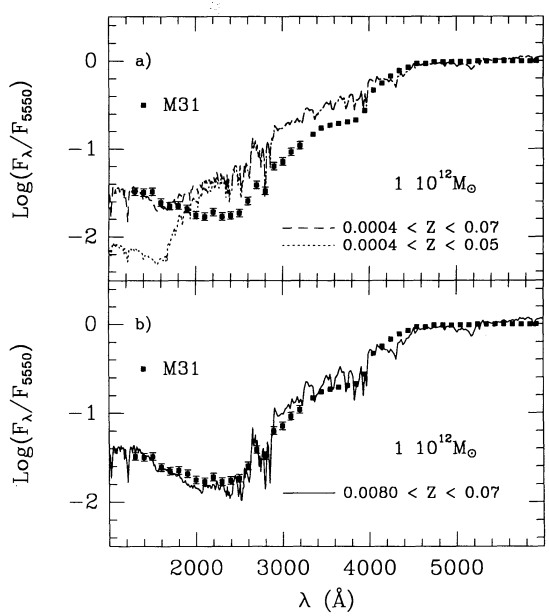

FIG. 5.—Comparison between the observed SED of M31 (*filled squares*) with three synthetic models for a galaxy mass of 10^{12} $M_\odot$ and different abundance distribution (from Bressan et al. 1994). The theoretical SEDs have been reddened adopting a value $E_{B-V} = 0.08$. The error bars represent the uncertainty (0.04 dex) of the *IUE* data. (*a*) Pure closed-box model (*dashed line*) and the same model excluding stars with metallicity higher than $Z = 0.05$ (*dotted line*). (*b*) The same model computed by imposing a lower cutoff ($Z = 0.008$) to the metallicity (*solid line*).

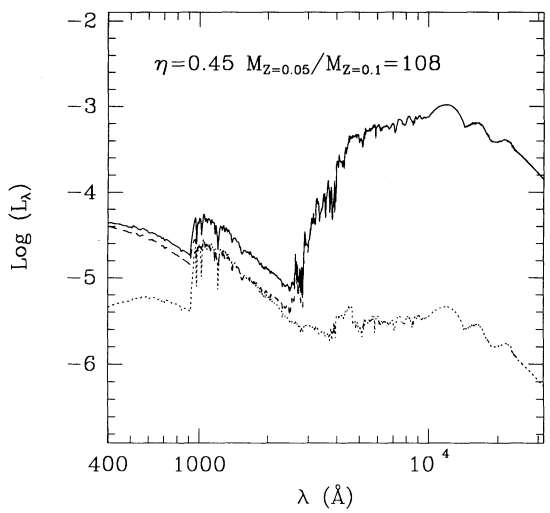

FIG. 6.—SEDs of the SSPs with age of 13×10^9 yr. The dotted line is the SED for the metallicity $Z = 0.1$, in which the UV upturn is dominated by the contribution from H-HB and AGB-manqué stars. The dashed line is the SED of the SSP with metallicity $Z = 0.05$, in which the UV upturn is generated only by P-AGB stars. The SEDs are for total mass in stars equal to 1 $M_\odot$. The two SEDs are scaled so that coincidence at 1000 Å is achieved and then summed up to generate the composite SED (*solid line*). The scaling factor represents the ratio of the mass stored in the metal-rich and normal metal content populations in order to get a composite SED obeying the constraints imposed by the count rate in the UV range of the SED for M31. See the text for a detailed discussion of this diagram.

SSP with $Z = 0.1$. To mimic the results of § 4.2.1, the fluxes of the two SSPs are scaled in such a way that they coincide at about $\lambda = 1200$ Å. This means that the two SSPs equally contribute to the total flux in the region 1200–2200 Å, but that the $Z = 0.05$ SSP totally dominates the SED for $\lambda > 3000$ Å.

If we add these two SSPs, scaled in this manner, the result is the solid line drawn in Figure 6, which as $1550 - V = 3.3$, i.e., close to that of the model in § 4.2.1. As the original SED of each SSP is given in units of $M_\odot$, the scaling factor between the two SSPs is simply the ratio of the corresponding masses required to get the same amount of flux from the P-AGB stars and the P-EAGB, H-HB, and AGB-manqué stars. Assuming the Salpeter initial mass function (IMF) with the lower limit at 0.1 $M_\odot$, the scaling factor $M_{Z=0.05}/M_{Z=0.1}$ is 108. In other words, about 1% of very metal-rich stars can generate the same amount of flux as the remaining 99% stars with normal metal content.

Closer examination of the properties of the UV sources reveals why this is so. Passing from P-AGB stars to P-EAGB, AGB5-manqué and H-HB objects, both the luminosity and mean effective temperature decrease, whereas the lifetime increases. While the lifetime of the brightest P-AGB stars is only a few 10^4 to 10^5 yr, it increases to about 10^6 yr and a few 10^6 for the fainter P-EAGB and AGB-manqué stars, respectively, and finally becomes as long as a significant fraction (up to 50%) of the core He-burning lifetime ($\sim 10^8$ yr) for the much fainter H-HB stars. As will be explicitly shown below (§ 4.2.3), the mean UV luminosities of individual P-AGB stars on the one hand, and of P-EAGB, H-HB, and AGB-manqué stars on the other hand, are within a range of 5 mag, with the P-AGB and H-HB stars at the brightest and faintest ends, respectively, and the P-EAGB somewhere in between. Hence, the numerical superiority of P-AGB stars is countered by the longer lifetimes of the P-EAGB, H-HB, and AGB manqué stars such that the high-metal stars produce proportionally far more UV flux than the lower metal stars. As shown in Figure 6, this interpretation does not affect the interpretation of the optical SED of a galaxy, as the high-metal stars contribute a negligible amount of flux beyond 3500 Å.

Separately we note that, with this simple composite model, we also satisfy the SED constraint placed on the M31 stellar population by the HUT observations of Ferguson & Davidsen (1993): The composite model has decreasing flux from 1000 Å to the Lyman limit at 912 Å. This is not unexpected, as Ferguson & Davidsen (1993) pointed out that to fit this decline one needs a composite spectrum.

4.2.3. *M31 UV CMDs*

The SSP models of § 4.2.2 can be directly applied to observations of M31 via CMDs using the F150W observations presented here combined with the F175W observations of King et al. (1992).

We have already noticed in § 2.2.3 that the nominal King et al. (1992 efficiency curve $\Gamma^N_{17}(\lambda)$ is not fully satisfactory since it does not reproduce the observed ratio of counts for the 48 stars we have in common with King et al. (1992). There are also two additional discrepancies when using $\Gamma^N_{17}(\lambda)$. The total number of counts within our *IUE* aperture given by King et al. (1992) is 256, whereas the predicted one is 192 (Table 5C). This discrepancy can be lowered by choosing a slightly higher background level, but not eliminated. Finally, with our adopted curve we obtain that the resolved stars contribute to the 51% of the total

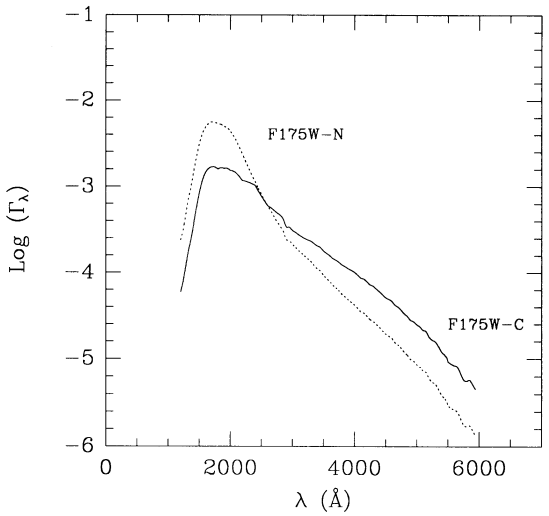

FIG. 7.—Nominal (F175W–N) and corrected (F175W–C) efficiency curves $\Gamma_{17}(\lambda)$ of the passband F175W used by King et al. (1992). See the text for more details.

UV (1200–2450 Å) light. On the contrary, this fraction is only 14% in the case of King et al. (1992) using their $\Gamma^N_{17}(\lambda)$. We were able to consistently eliminate the above discrepancies by assuming a new efficiency curve for King et al. (1992) observations slightly depressed in the UV region and with a higher redleak. This curve, which we term $\Gamma^C_{17}(\lambda)$, is compared to the nominal one $\Gamma^N_{17}(\lambda)$ in Figure 7.

With this new curve the ratio between the predicted counts for the 48 stars in common with King et al. (1992) becomes 1.2 (King et al. vs. this paper), in fair agreement with the measured ratio of 1.47. In addition, the predicted number of counts is 254, very close to the measured one (Table 5D). Finally, the contribution of the resolved stars to the UV light is 40%, in agreement with our estimate. It is clear that the modified curve $\Gamma^C_{17}(\lambda)$ suffers from a certain degree of arbitrariness as it is not unique. Furthermore it has been suggested on the basis of our own calibration and not on the basis of internal inconsistencies in the King et al. (1992) observations. However, it seems reasonable to us to adopt such a curve in the following discussion of the CMDs. It should be noted that our modification of $\Gamma^N_{17}(\lambda)$ is primarily formal rather than substantial.

In the following CMDs we plot m_{15} versus $m_{15} - m_{17}$. These colors are obtained adding a constant factor of 8.41 to magnitude m_{17} of King et al. (1992) in order to take into account the different zero point of the magnitude scale. The CMDs are generated by adopting the corrected $\Gamma^C_{15}(\lambda)$ and $\Gamma^C_{17}(\lambda)$ efficiency functions. We will also discuss the relevant effects if the nominal efficiency curves are used for these two passbands.

For the following analysis, SSP isochrones are generated with lifetimes of 13×10^9 yr and typical chemical compositions of $Y = 0.280$ and $Z = 0.020$ (i.e., solar) and $Y = 0.475$ and $Z = 0.1$. Isochrones of younger (but still relatively old) SSPs have a similar shape even if they may differ in the maximum luminosity reached by the AGB stars (see the calibration in Bressan et al. 1994 for more details).

The theoretical magnitudes and colors are translated into the observational ones by assuming the intrinsic distance modulus to M31 of $(m - M)_0 = 24.20$ (Freedman 1989, 1992), and the extinctions $A_{15} = 0.66$ and $A_{17} = 0.62$ derived from

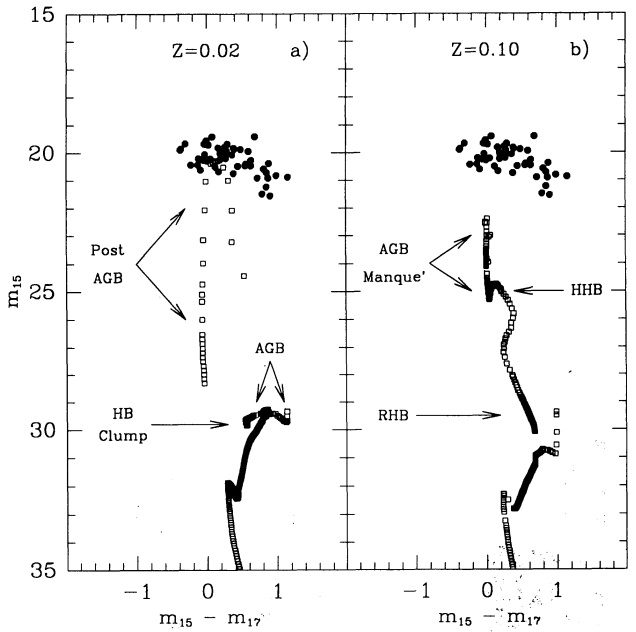

FIG. 8.—Isochrones in the CMD m_{15} vs. $m_{15} - m_{17}$ for two metallicities, (*a*) $Z = 0.2$ and (*b*) $Z = 0.10$. The age is 13×10^9 yr. The filled dots are the colors of the stars of M31 in common with King et al. (1992). The theoretical magnitudes and colors are obtained with the corrected efficiencies $\Gamma^C_{15}(\lambda)$ and $\Gamma^C_{17}(\lambda)$. The absolute theoretical magnitudes are translated into apparent values assuming $(m - M)_0 = 24.2$ and reddening $A_{15} = 0.66$ and $A_{17} = 0.62$ derived from the Cardelli et al. (1992) law with $E_{B-V} = 0.08$. The horizontal arrows in (*b*) indicate the regions of stationary He-burning as cool HB (*bottom*) and H-HB stars (*top*). See the text for more details.

the Cardelli, Clayton, & Mathis (1992) law with $E_{B-V} = 0.08$ (Burstein & Heiles 1984). The reader should note that the density of model points along the isochrones drawn in the CMD figures is *not* proportional to the lifetimes of the underlying evolutionary phases. Hence, these figures are not intended for use in inferring the luminosity functions of hot stars.

The CMDs for the corrected efficiency curves are shown in Figures 8*a* and 8*b*, together with the magnitudes and colors for individual stars detected in both the F150W and F175W images. The morphology of these SSPs is analogous to that seen in capital CMDs, albeit quite condensed owing to the close UV bandpasses used. The evolved portions of the isochrones corresponding to the RGB and AGB phases of normal-metallicity stars (Fig. 8*a*) are redder than the main sequence, while as expected the H-HB and AGB-manqué stages (Fig. 8*b*) of the high-metallicity case are somewhat bluer than the main sequence. For metallicity $Z = 0.02$ the brightest part of the isochrone matches well both the m_{15} magnitudes of the observed stars and the mean $m_{15} - m_{17}$ colors of these stars. In contrast, for stars with $Z = 0.1$, the whole isochrone remains at least 2 mag fainter than the observed stars.

For $Z = 0.02$ the brightest part of the isochrone in Figure 8*a* corresponds to the P-AGB stages, with evolution for P-AGB stars proceeding from right to left in this diagram. For $Z = 0.1$ the brightest stars in Figure 8*b* correspond to the P-EAGB and AGB-manqué stages, with H-HB stars defining the fainter distribution as indicated.

For the large majority of our detected stars (included those in common with King et al. 1992, shown in Figs. 8*a* and 8*b*) one can infer a detection limit of $m_{15} \sim 22$. Therefore, while the brightest P-AGB stars with $Z = 0.02$ are above detection, the metal-rich P-EAGB, H-HB, and AGB-manqué stars with $Z = 0.1$ fall below this, thus presumably contributing only the bulk of the count rate to the background on these images.

The observations have a wider spread in color than is given by the simple SSP. Part of this spread is due to errors of observation. Rough estimates of the measurement errors yield $\Delta m_{15} \simeq 0.3$ and $\Delta m_{17} \simeq 0.2$. Separately, the error in the zero level of the color has an uncertainty of about 0.5 mag. Part of the spread is also undoubtedly due to the stars having a range of initial metallicity and possibly age.

A preliminary analysis of this leads to the following dependence of the magnitude m_{15} of the brightest part of the isochrones in the m_{15}-$(m_{15} - m_{17})$ plane as a function of the age and metallicity,

$$m_{15} = 15.89 - 1.6 \log Z + 1.75 \log t_9 , \qquad (4)$$

where t_9 stands for the age in units of 10^9 yr. The range of validity is $Z \leq 0.05$ and $\log t_9 \geq 0.4$. The sources are all P-AGB stars. At a given age, stars get brighter with increasing metallicity. Conversely, at a given metallicity stars get brighter with decreasing age. For metallicities greater than $Z = 0.05$, the above relation breaks down and the trend is no longer monotonic. In brief, for ages younger than approximately $\log t_9 = 0.7$ and $Z > 0.05$, the magnitude m_{15} of most luminous UV emitters (of P-AGB type) gets brighter with increasing metallicity and age. In contrast, for ages older than $\log t_9 = 0.7$ and $Z > 0.05$, the opposite occurs; the m_{15} magnitude of the UV source (now of H-HB and AGB-manqué type) gets fainter with increasing age and metallicity. It follows that, unless the population of UV emitters is both very metal-rich and young, only the PAGB stars will be represented among the UV-brightest stars, while all other types of UV-bright old stars would be fainter than $m_{15} = 22$ and hence undetectable with our current observations.

The magnitude range spanned by the observational data (see Figs. 2 and 8) perhaps suggests that a correponding spread in metallicity (and possibly in age) of about 50% is present. On this basis, we would conclude that the models fit the observations surprisingly well within both model and observational constraints.

What would have happened if we made this comparison using the nominal efficiency for the F150W and F175W images, Γ^N_{15} and Γ^N_{17}? In this case, the brightest P-AGB stars would be predicted to be over 1.5 mag brighter and about 1 mag bluer than the stars observed. Thus the nominal efficiencies are inconsistent with the models at 7 σ for the mean apparent magnitude and about 3 σ for the mean color. An intermediate result would, of course, emerge if we intermixed nominal and corrected efficiencies for these two images.

4.2.4. *Luminosity Functions of the UV Sources in M31*

Of the three galaxies in our survey, only M31 both has a large enough number of detected stars and is suspected to be of sufficiently old age that comparisons of model old-star luminosity functions to the observations are warranted. In Figures 9*a* and 9*b* we plot the luminosity function in m_{15} for M31 stars (*dashed lines*) together with the values predicted for the two SSPs discussed in § 4.2.3: $Z = 0.02$ (Fig. 8*a*) and $Z = 0.1$ (Fig. 8*b*). The model luminosity functions for M31 hot stars (i.e., the number of hot stars per magnitude interval m_{15} at the M31 distance) are calculated for the corrected efficiency, $\Gamma^C_{15}(\lambda)$, and the Salpeter initial mass function with the same normalization constant.

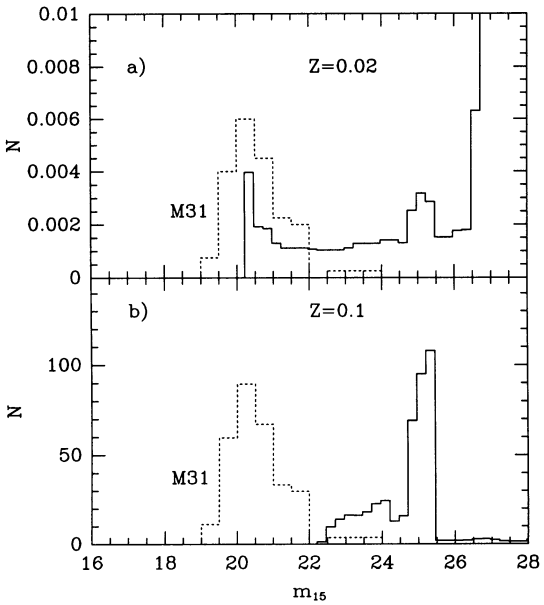

FIG. 9.—Theoretical luminosity functions (m_{15} magnitude) corresponding to SSPs with age of 13×10^9 yr and different metallicities: (*a*) $Z = 0.02$ and (*b*) $Z = 0.10$. The adopted scales reflect the different lifetimes of the evolutionary phases contributing to the UV emission, as detailed in the text. The luminosity functions (*solid lines*) are calculated for the corrected $\Gamma_{15}(\lambda)$. The observational luminosity function of M31 (*dotted line*) is superimposed (without normalization) for illustration purposes.

Solar metallicity stars ($Z = 0.02$) in the P-AGB phase are characterized by a minor clump of bright objects centered at about $m_{15} = 20.5$, followed by a long tail extending to $m_{15} = 25$, while the bulk of the distribution is fainter than this (at $26.5 < m_{15} < 28.5$). The luminosity function for metal-rich stars is characterized by several groups: There is a small fraction of bright P-EAGB and AGB-manqué stars that have maximum luminosities 1.5 mag fainter ($m_{15} \sim 22.5$) than the brightest $Z = 0.02$ P-AGB stars. These merge with the group of H-HB stars located at $24.5 \leq m_{15} \leq 25.5$). Finally, there is the peak of the cool HB stars at $m_{15} > 29$ (these are not displayed in Figs. 9*a* and 9*b*).

It is worth pointing out that since the two theoretical luminosity functions displayed in Figures 9*a* and 9*b* are calculated with the same normalization constant in the initial mass function, the very different number of stars per magnitude bin mirrors the different duration of the underlying evolutionary phases.

Finally, as with the CMDs, use of the nominal efficiency for the F150 + F130LP filter combination would predict luminosity functions which are about 1.5 mag brighter.

4.2.5. *UV Sources in M31*

The models of Bressan et al. (1994) show in several different ways that the stars actually observed in our FOC f/48 F150W + F130LP image of M31 are primarily P-AGB stars, with perhaps a small contribution from the brightest possible P-EAGB stars. These resolved stars appear to contribute about 50% of the total integrated flux in this image within the *IUE* aperture of 154 arcsec^2. Based on these models, we would predict that the other 50% of the observed counts in M31 come from P-EAGB, H-HB, and AGB-manqué stars that are not resolved in this image.

Ferguson & Davidsen (1993) have pointed out that the UV spectra of elliptical galaxies are probably composite, with the ratio of hot UV stars ($T_{\rm eff} \sim 30{,}000$ K) to cooler UV stars ($T_{\rm eff} \sim 24{,}000$ K) being a decreasing function of the mean metallicity of the stellar population. The models calculated here give a plausible interpretation to the physics behind this correlation: The most metal-rich galaxies (or older galaxies?; see § 5), such as NGC 1399, have their UV flux dominated by P-EAGB, H-HB, and AGB-manqué stars, which the models show tend to be of lower temperature than P-AGB stars. As the mean metallicity of the stellar population decreases, the ratio of P-AGB to P-EAGB + H-HB + AGB-manqué stars increases, and the mean temperature of the UV-hot stars increases.

4.3. *Hot Stars in NGC 205*

The ground-based data for NGC 205 has been recently discussed by Peletier (1993). Since the early studies by Baade (1951), this galaxy has long been considered to show evidence of ongoing star formation because of the UV-bright stars as well as the large number of regions of absorption and dust (Hodge 1973). Mould, Kristian, & da Costa (1983, 1984) determined a metallicity $[M/H] = -1.2 \pm 0.2$ from the CMD in the outer regions. Peletier (1993) studied the color profile of the galaxy and found a very blue center and colors that get redder slowly going outward. Because of the presence of blue luminous stars in the center, the color gradient is interpreted as a gradient primarily in age. The existence of luminous OB stars sets a limit to the age of the most recent episode of star formation in NGC 205 at a few 10^6 yr. Furthermore, the galaxy contains a number of bright red stars, which are so bright that they either are red supergiants or evolved AGB stars (Gallagher & Mould 1981).

Following Peletier (1993), NGC 205 can be modeled as having old stars with some young stars in the center. The age of the underlying old component is difficult to assess. The study of Mould et al. (1983, 1984) implies an age not younger than a few 10^9. Using the static population synthesis technique, Bica, Alloin, & Schmidt (1990) inferred from the UV/optical SED the existence of an old component whose metallicity lies in the range $-2 \leq Z/Z_\odot \leq -1$, and whose age is older than 5×10^9 yr, perhaps as old as $(12\text{–}13) \times 10^9$ yr. Bica et al. (1990) also inferred the existence of a young component with age in the range 10^7 to a few 10^8 yr, which contributes to about 80% of the visible light.

On the basis of these observations, the stellar population of NGC 205 is reasonably modeled in terms of the evolutionary stellar population models of Bressan et al. (1994). The young stars in NGC 205 are modeled with a burstlike episode at constant rate whose duration is from 5×10^8 yr ago to the present time, say a few 10^6 yr. This young burst is superimposed on an exponentially decreasing star formation rate that was maximal 13×10^9 yr ago. The exponential timescale for decrease of star formation is taken to be about 1×10^9 yr, so that essentially no stars are currently formed from this initial mode. The amplitude of star formation in the young burst with respect to that in the older phase is chosen in such a way that the relative total mass of stars born in the two episodes are matched. Some experimentation with the models shows that although the young burst population dominates the visible light, it contains only about 2% of the total mass of stars in the NGC 205.

To simulate our CMDs we have adopted a simple law of metal enrichment according to which, as the galaxy ages, the

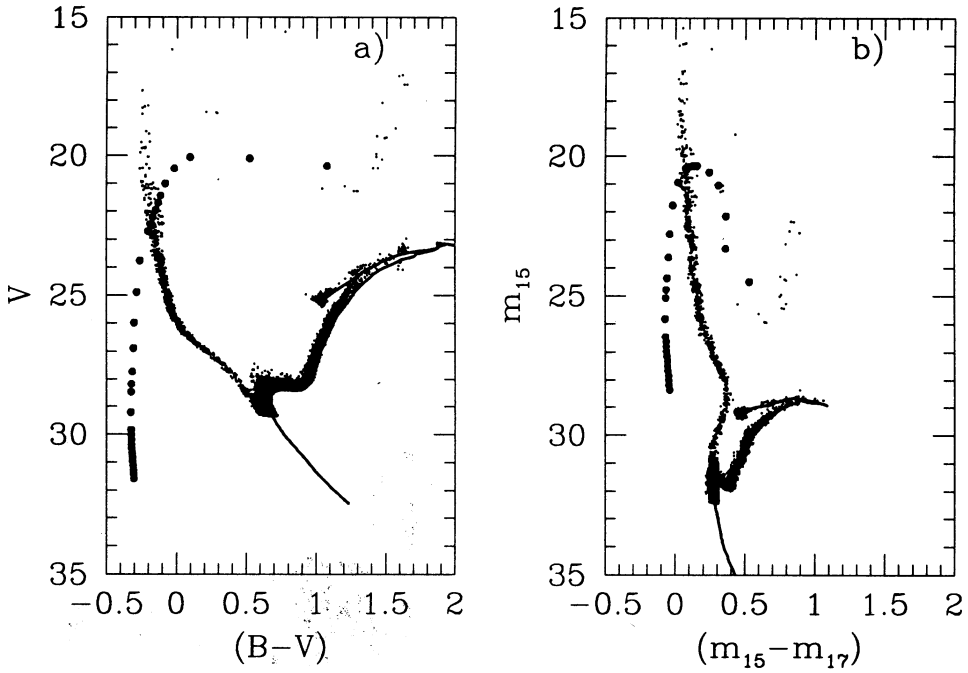

FIG. 10.—Two simulated CMDs for the galaxy NGC 205: (*a*) is the classical V-$(B-V)$ CMD, while (*b*) is for the m_{15}-$(m_{15}-m_{17})$ plane. The simulations are obtained assuming that star formation began 13×10^9 yr ago, underwent an exponential decline with a typical *e*-folding time of 1×10^9 yr, and suffered from a recent burst of constant strength 5×10^8 yr ago. The ratio of the exponential star formation generating the old component to the burst producing the young stars is such that the total mass of the latter is about 2% of the former. In the course of evolution, the metallicity increased linearly from $Z = 0.0004$ to $Z = 0.008$. The P-AGB stars are indicated by filled circles. Both VMDs are in apparent magnitudes having assumed $(m - M)_0 = 24.7$ and $E_{B-V} = 0.035$. See the text for more details. It is evident that the number of P-AGB stars in the observed sample can amount to 1%–2%, at most. All remaining stars are young objects.

composition varies linearly with time from $Y = 0.23$ and $Z = 0.0004$ to $Y = 0.25$ and $Z = 0.008$. This keeps the overall metallicity of the old stars in accord with the observations that mean metallicity is [Fe/H] ~ -1.5. Figure 10 shows the synthetic M_V versus $(B-V)_0$ diagram, while Figure 10*b* shows the m_{15} versus $m_{15} - m_{17}$ diagram, along the same precepts as produced for the corrected efficiency curves for M31 data. Each CMD has been plotted assuming a distance modulus of NGC 205 of $(M - m)_0 = 24.7$ (Price & Grasdalen 1983) and a color excess $E_{B-V} = 0.035$ (Burstein & Heiles 1984). In both diagrams the simulations are magnitude limited, in the sense that the only stars plotted are above the main sequence turnoff. The location of fainter stars is approximated by the isochrone of 13×10^9 yr.

In both diagrams the young population (younger than 5×10^8 yr) is clearly distinct from the old one. The classical $B-V$ CMD shows the expected distributions of stars in the various phases of evolution, and there are no special features to be remarked upon. In contrast, the m_{15} versus $m_{15} - m_{17}$ CMD deserves several comment. As expected, all evolutionary stages but that for the P-AGB stars are significantly fainter than the younger stars. P-EAGB, H-HB, and AGB-manqué stars are not present owing to the low metallicity found for this galaxy, from which only P-AGB stars are expected to be produced. Evolved red stars, either red supergiants or intermediate age AGB stars, are much fainter than both the young, blue stars or the brightest P-AGB stars.

The lifetimes of P-AGB stars from the older population (few 10^4 yr) are 100–10,000 times shorter than those of the main-sequence OB stars (few 10^6 yr to 10^8 yr). Hence, even if the P-AGB stars were of the same luminosity as the OB stars, they would not contribute much to the total UV flux in NGC 205. The predicted location and numbers of P-AGB stars are shown in Figure 10 as closed circles. Based on these calculations, it is estimated that fewer than two out of 100 UV-bright stars could be old P-AGB stars. Essentially all of the hot stars in NGC 205 observed in our FOC image were formed in the more recent starburst episode.

Comparison of the theoretical luminosity function with the observed luminosity function would not yield much useful information in the absence of knowledge of the individual ages of the young stars. However, it is worth noting that the relatively flat UV/optical SED (Fig. 3) is due to both (1) that the optical SED is a combination of old and young stellar light and (2) that the young stars are aging and a strong population of O stars does not dominate the UV continuum.

4.4. *Hot Stars in M32*

The optical/near-infrared stellar content of M32 has been examined in great detail by Freedman (1989, 1992) and Bressan et al. (1994) to whom the reader is referred. Briefly, this galaxy is best modeled by a prominent burst of activity at 13×10^9 yr, followed by a recent episode that occurred not earlier than say (2–5) $\times 10^9$ yr ago. The mean metallicity of stars in M32 is significantly more metal rich than that of stars in NGC 205 (see Bressan et al. 1994 for a thorough discussion of this point). However, what was learned from the simulation of the star formation history for NGC 205 can also be applied to the case of M32. The result of such an analysis is fairly obvious: Lacking ongoing star formation and strong UV excess (this latter excludes very high metallicities), the low UV flux is most likely generated by P-AGB stars.

Here also we do not make explicit comparisons to the observed m_{15} luminosity function of M32, as only 10 stars is

too few on which to base any statistically significant interpretation.

5. SUMMARY AND CONCLUSIONS

In this paper we present UV observations of the nuclear regions of the M31, M32, and NGC 205 obtained with the *HST* FOC in the f/48 optical train and the combination of the UV filters F150W and F130LP. The absolute calibration of the data is tricky, as it involves resolving an internal disagreement between observed and expected count rates in the UV. A corrected efficiency curve for our observations is developed using *IUE*-based UV/optical spectral energy distributions for these galaxies and is checked in two different ways, including a direct comparison of stellar count rates for stars observed in common with the FOC F175W observations, of King et al. (1992). The significant differences between the nominal efficiency curve and the corrected efficiency curve derived here lead us to suggest that the filter combination of F150W + F130LP suffers from a degraded UV sensitivity which could be attributed to either filter or to both.

Of the three galaxies, only M31 is found to have both a significant number of detected stars (81) as well as a strong, unresolved background. The complicated structure of the nucleus of M31 as seen by Lauer et al. (1993) is confirmed, but the UV flux from this nucleus as well as the individual stars cannot be strictly derived from the present data as it is affected by a substantial amount of redleak. Even if proper ground-based longer wavelength observations of our FOC field could constrain this effect, the present ambiguity will be fully removed only by means of future *HST* observations making use of proper filters such as the Woods F160W filter, with essentially no redleak beyond 2500 Å. However, based on comparisons with the FOC F175W data of King et al. (1992) and optical images, we find that all of the detected stars are consistent with hot stars. Comparing the count rate from the stars to the less accurate estimate of UV flux actually measured (using the corrected efficiency curve), these resolved stars could contribute to about 50% of the UV flux between 1200 and 2450 Å. This requires a model that can provide both a relatively small number of bright hot stars and a large number of fainter hot stars.

Analysis of these data is done with the isochrones and theoretical SEDs from the Bertelli et al. (1994) and Bressan et al. (1994) libraries, respectively, and the aid of simulations of the CMDs in the UV passbands. In this analysis we also made use of the data for M31 obtained by King et al. (1992) in the F175W passband, according to which the flux in resolved stars amounts to about 75% of the total. However, we notice that an internal inconsistency similar to that found for the F150W + F130LP passband could also affect the F175W passband. We propose a modified efficiency curve for this filter that not only removes the above internal inconsistency but also reconciles King et al.'s (1992) results with ours.

The theoretical models calculated here show that a minority stellar population of very metal-rich old stars ($Z > 0.05$) can produce hot stellar progeny (P-EAGB, AGB-manqué, and H-HB stars) that are of somewhat lower UV luminosity but of longer lifetimes than the P-AGB stars produced by lower metal, low-mass stars. Furthermore, the simulations of the CMDs and luminosity functions in the m_{15} and m_{17} passbands clearly show that the detected stars are most likely the P-AGB objects belonging to the stellar component of normal metallicity. All remaining sources of UV-flux (P-EAGB, AGB-manqué, and H-HB stars) that are required to account for the count rates and shape of the UV side of SEDs fall below detection.

A variation in the ratio of very metal-rich stars to stars of lower metallicity as a function of the mean metallicity of a stellar population can plausibly produce the change in mean temperature of the stars as a function of metallicity, as observed by Ferguson & Davidsen (3993) between M31 and NGC 1399. The models examined here also suggest that $\sim 50\%$ of the observed UV flux in M31 should come from resolved stars, consistent with what is observed.

In this context, we would like to comment on how the above scenario conforms with the recent results by Gonzalez (1993) on the age range spanned by elliptical galaxies. The correlation between the Hβ and [MgFe] index derived from the theoretical analysis by Worthey (1992) seems to indicate that galaxy ages vary from say (12–15) $\times 10^9$ yr for objects like NGC 4649 and NGC 7619 down to the age of 3×10^9 yr for galaxies like NGC 221 (M32) and NGC 1700. If this age range is real, could it be that age rather than metallicity determines the nature and efficiency of the UV sources? Or both in suitable proportions? Answering these questions is a cumbersome affair requiring full exploration of the parameter space ($\Delta Y/\Delta Z$, metallicity, and age) not yet abailable. On the base of the $(1550 - V)$-age-metallicity calibrations for SSPs of Bressan et al. (1994) and Fagotto (1994), the age cannot be the sole parameter because a minimum metalicity (depending on the adopted $\Delta Y/\Delta Z$ and mass-loss rates) is required to generate SEDs able to match the constraints imposed by the correlation between the UV-flux and Mg_2 index and the HUT observations of Ferguson et al. (1991) and Ferguson & Davidsen (1993). Conversely, if this metallicity is reached, the age can drive the intensity of the UV flux, younger galaxies having lower UV emission. The dependence of the UV excess—as measured by the color $1550 - V$—on age, metallicity, and $\Delta Y/\Delta Z$ ratio has been investigated by Fagotto (1994) using $\Delta Y/\Delta Z = 2.5$ and $\Delta Y/\Delta Z = 3.5$. As expected, with increasing $\Delta Y/\Delta Z$, the onset of P-AGB, H-HB, and AGB-manqué stars in a stellar population starts at lower metallicities and younger ages, and more relevant, the color $1550 - V$ smoothly gets stronger with increasing age. Older (and likely more metal-rich) galaxies having more numerous P-EAGB, H-HB, and AGB-manqué stars would possess stronger UV excess, the opposite for younger galaxies. In relation to this, the results of Faber et al. (1992), Gonzalez (1993), and Worthey (1992) could be framed in a more general context in which age, metallicity, and history of metal enrichment ($\Delta Y/\Delta Z$) concur to determine the UV properties of elliptical galaxies. However, a fully satisfactory answer to the fundamental problem of the age spread among elliptical galaxies requires a much deeper analysis of the relation between age, metallicity, UV excess, line-strength indexes, and absolute luminosity of these systems.

All of the observed UV flux in NGC 205 can be accounted for by the observed stars; no diffuse background is detected. Much of the UV flux from NGC 205 comes from its very blue nucleus. This nucleus is slightly resolved on our image, and its brightness and size implies it is produced by ~ 10 OB stars.

Only 10 individual stars are detected in M32, consistent with its low UV flux. Almost all of the flux from M32 comes from the unresolved background, which appears smooth and elliptical in shape. These data are compatible with the general interpretation that the mean metallicity of the stellar population of M32 is somewhat less than solar and/or its stellar

population substantially younger than that of M31. As also discussed by Bressan et al. (1994), low metallicity alone would imply that M32 would have few stars with $Z > 0.05$, resulting in much lower overall UV flux for this galaxy.

We would like to thank I. R. King, P. Crane, and G. De Marchi for useful discussions. I. R. King and P. Crane kindly supplied us with useful information and FOC data in advance of publication. This study has been financially supported by the Italian Ministry of University, Scientific Research and Technology (MURST) and the Italian Space Agency (ASI). Support for this work was provided by NASA to D. B. through grant GO-2719.01-87A from the Space Telescope Science Institute, which is operated by the Association of Universities for Research in Astronomy, Inc., under NASA contract NAS 5-26555.

REFERENCES

Baade, W. 1951, Publ. Univ. Michigan Obs., 10, 7
Bertelli, G., Bressan, A., Fagotto, F., Chiosi, C., & Nasi, E. 1994, A&AS, 106, 275
Bertelli, G., Chiosi, C., & Bertola, F. 1989, ApJ, 339, 889
Bertola, F., Capaccioli, M., Holm, A. V., & Oke, J. B. 1980, ApJ, 237, L65
Bertola, F., Capaccioli, M., & Oke, J. B. 1982, ApJ, 254, 494
Bertola, F., Gregg, M. D., Gunn, J. E., & Oemler, A., Jr. 1986, ApJ, 303, 624
Bica, E., & Alloin, D. 1987, A&A, 186, 49
———. 1988, A&A, 192, 98
Bica, E., Alloin, D., & Schmidt, A. 1990, A&A, 228, 23
Bohlin, R. C., & Holm, A. V. 1980, NASA *IUE* Newsletter, 10, 37
Bressan, A., Chiosi, C., & Fagotto, F. 1994, ApJS, 94, 63
Bruzual, G. A. 1983, ApJ, 273, 205
Burstein, D., Bertola, F., Buson, L. M., Faber, S. M., & Lauer, T. R. 1988, ApJ, 328, 440
Burstein, D., & Heiles, C. 1984, ApJS, 54, 33
Buson, L., Bertola, F., Burstein, D. 1990, in Windows on Galaxies, ed. G. Fabbiano, J. Gallagher, Jr., & A. Renzini (Dordrecht: Springer-Verlag), 51
Cardelli, J. A., Clayton, G. C., & Mathis, J. S. 1989, ApJ, 345, 245
Castellani, M., & Tornambé, A. 1991, ApJ, 381, 393
Chiosi, C., Bressan, A., Vallenari, A., & Ortolani, S. 1994, A&A, in preparation
Code, A. D., & Welch, G. A. 1979, ApJ, 228, 95
De Marchi, G., Paresce, F., & Ferraro, F. R. 1993, ApJS, 85, 293
Dorman, B., Rood, R. T., & O'Connoll, R. W. 1993, ApJ, 419, 596
Faber, S. M., Gonzalez, J. J., & Worthey, G. 1992, in IAU Symp. 149, The Stellar Populations of Galaxies, ed. B. Barbuy & A. Renzini (Dordrecht: Kluwer), 225
Fagotto, F. 1994, in Stellar Populations, Mem. Soc. Astron. Ital., in press
Fagotto, F., Bressan, A., Bertelli, G., & Chiosi, C. 1994a, A&AS, 104, 365
———. 1994b, A&AS, 105, 39
Ferguson, H. C., & Davidsen, A. F. 1993, ApJ, 408, 92
Ferguson, H. C., et al. 1991, ApJ, 382, L69
Ford, H. C., & Jacoby, G. H. 1978, ApJS, 38, 351
Freedman, W. L. 1989, AJ, 98, 1285
———. 1992, AJ, 104, 1349
Gallagher, J. S., & Mould, J. R. 1981, ApJ, 244, L3
Gonzalez, J. J. 1993, Ph.D. thesis, Univ. California, Santa Cruz
Greenfield, P., et al. 1991, Proc. SPIE, 1494, 16
Greggio, L., & Renzini, A. 1990, ApJ, 364, 55
Hodge, P. W. 1973, AJ, 182, 671
Horch, E., Demarque, P., & Pinsonneault, M. 1992, ApJ, 388, L53
King, I., et al. 1992, ApJ, 397, L35
Kurucz, R. L. 1992, private communication
Lauer, T. R., et al. 1993, AJ, 106, 1436
Mould, H., Kristian, J., & da Costa, G. 1983, ApJ, 270, 471
———. 1984, ApJ, 278, 575
O'Connell, R. W. 1992, in IAU Symp. 149, The Stellar Populations of Galaxies, ed. B. Barbuy & A. Renzini (Dordrecht: Kluwer), 233
Oke, J. B., Bertola, F., & Capaccioli, M. 1981, ApJ, 243, 453
Paresce, F. 1992, in *HST* Faint Object Camera Instrument Handbook, Ver. 3, ed. F. Paresce (Baltimore: STScI)
Paresce, F., et al. 1991, Nature, 352, 297
Peletier, R. F. 1993, A&A, 271, 51
Price, J. S., & Grasdalen, G. L. 1983, ApJ, 275, 559
Rocca-Volmerange, B. 1989, MNRAS, 236, 47
Schönberner, D. 1983, ApJ, 272, 708
Sparks, W. B. 1991, Instrument Science Report FOC 53 (Baltimore: STScI)
Windhorst, R. A., & Keel, W. C. 1994, preprint
Wirth, A., Smarr, L. C., & Bruno, T. C. 1985, ApJ, 290, 140
Worthey, G. 1992, Ph.D. thesis, Univ. California, Santa Cruz